Advanced application of Thin Films part 2

Jari Koskinen

Function and utility

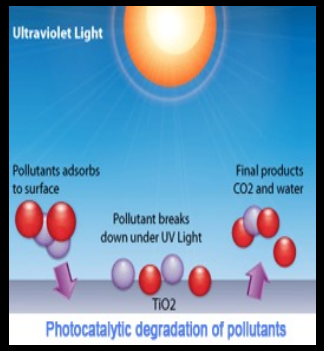

Titanium Dioxide: Photocatalytic activity

Indium Tin Oxide, ITO: Defrosting coating

Optical systems, optical MEMS

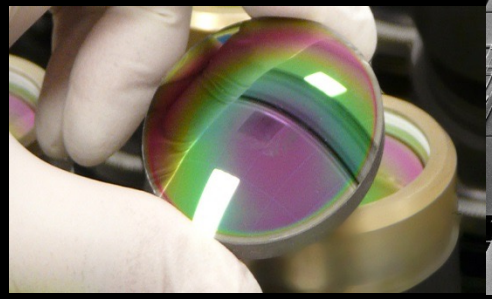

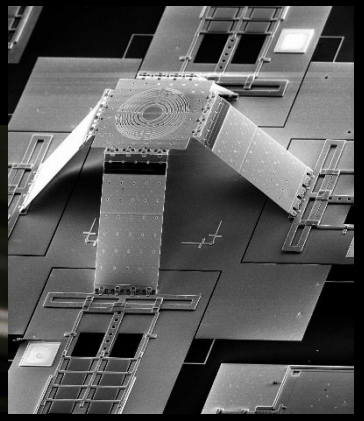

Microelectromechanical systems, MEMS

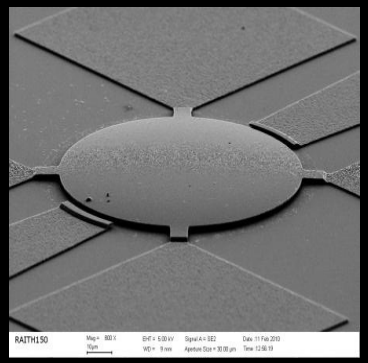

Part 2

- Energy harvesting (piezo)
- Optical coatings
  - Tunable transmission
- Magnetic Films for Data Storage
  - Magnetic discs
- Sensors
  - Gas sensors
  - Electro chemical sensors
- Photocatalytic TiO_2

Piezo thin films

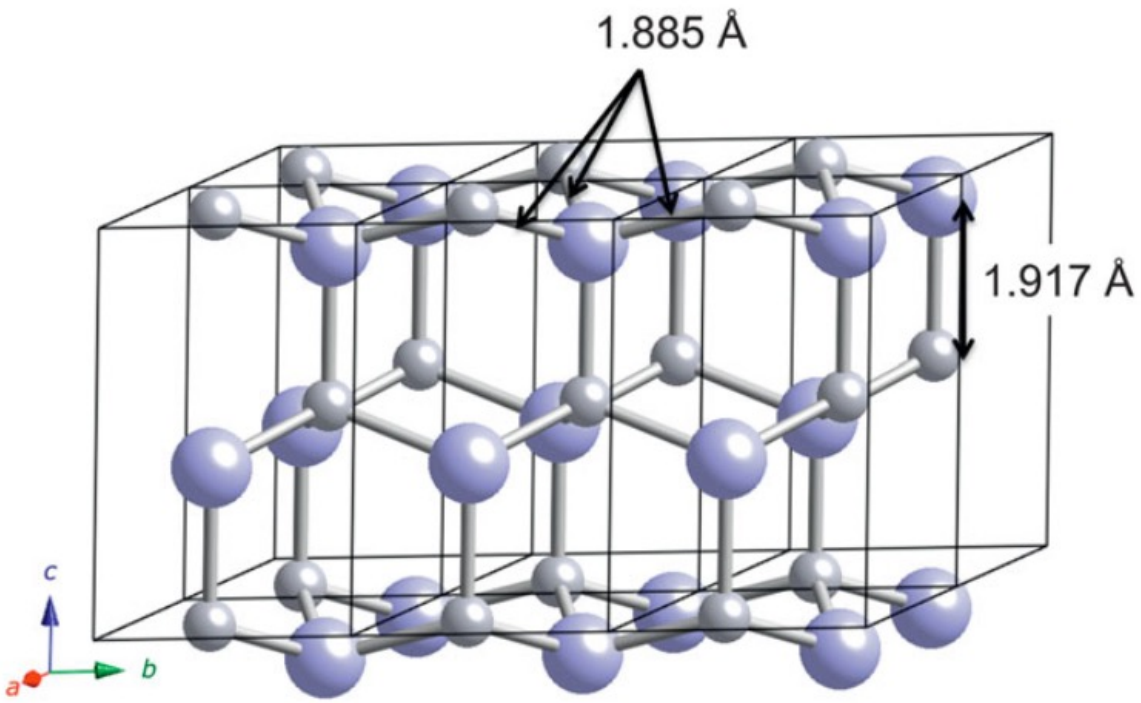

Figure 2. Wurtzite crystal structure of AlN showing Al atoms in gray and N in blue. All Al-centered tetrahedra are arranged with one neighbor directly above (parallel to the *c*-axis) and three neighbors forming the base of a pyramid below.

C. Eom, S. Trolier-McKinstry, MRS BULLETIN VOLUME 37 NOVEMBER 2012 www.mrs.org/bulletin

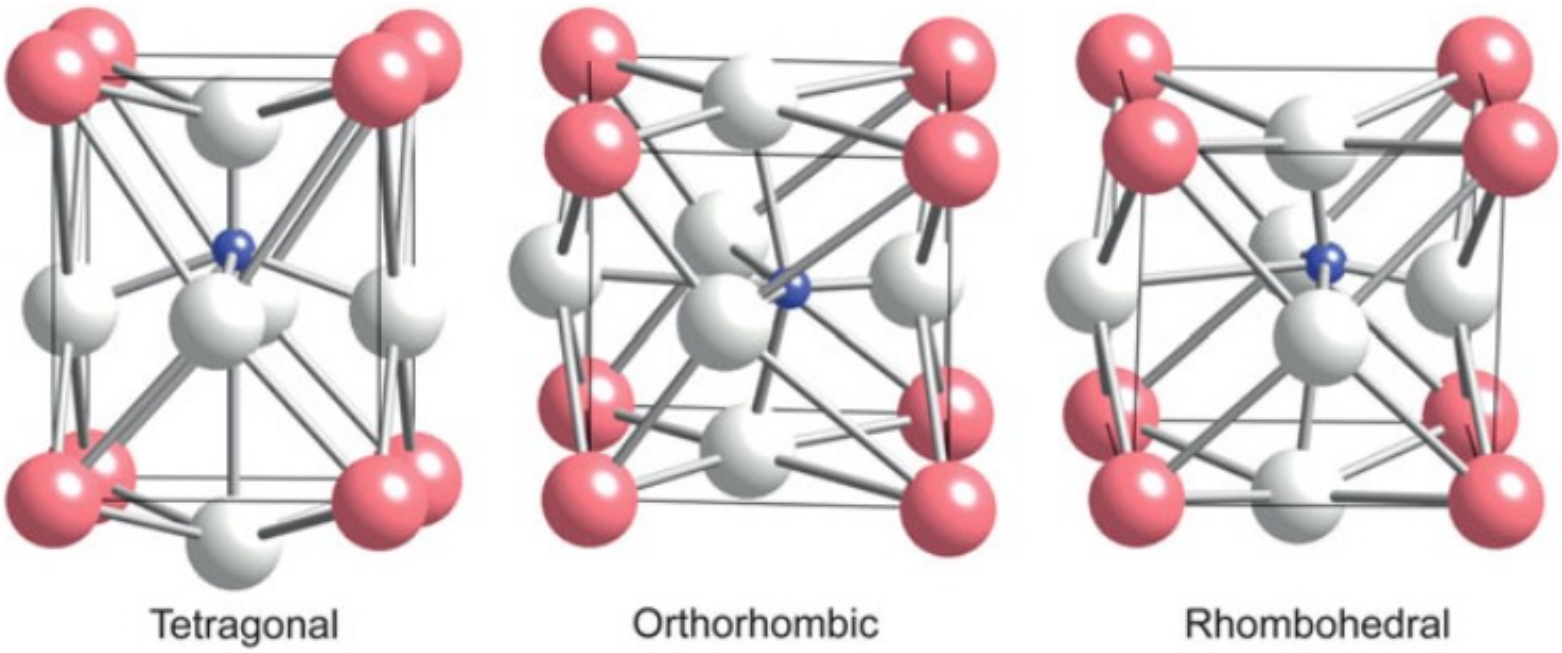

Figure 3. Typical ferroelectric distortions (exaggerated for clarity) of the perovskite ABO_3 structure; the A ions (red) are at the corners of the unit cell, the B ions (blue) are close to the center of the unit cell, and the O ions (white) are near the face centers. Upon developing spontaneous polarization, a spontaneous strain also develops.

C. Eom, S. Trolier-McKinstry, MRS BULLETIN VOLUME 37 NOVEMBER 2012 www.mrs.org/bulletin

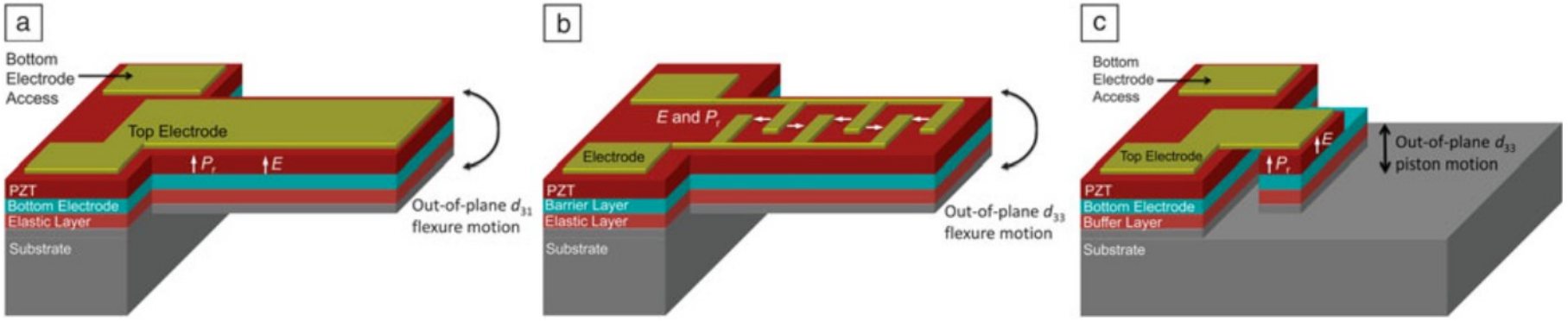

Figure 5. Illustration of common sensing and actuation modes in piezoelectric microelectromechanical systems. (a) Bending mode induced by $e_{31,f}$ (sometimes called d_{31} mode) for a film with top and bottom electrodes. The unimorph structure bends when lateral contraction of the piezoelectric layer acts on the passive elastic layer. (b) Out-of-plane bending due to in-plane expansion of d_{33} actuated-structure using interdigitated electrodes. In order to confine the electric field in the plane of the device, the layers underneath the piezoelectric should be electrically insulating. Barrier layers such as ZrO_2 or HfO_2 are typically required to prevent reaction between lead-based perovskites and Si or SiO_2 elastic layers. (c) Piston motion due to the out-of-plane d_{33} coefficient. Note: PZT, $Pb(Zr,Ti)O_3$; E, electric field; P_r, remanent polarization.

C. Eom, S. Trolier-McKinstry, MRS BULLETIN VOLUME 37 NOVEMBER 2012 www.mrs.org/bulletin

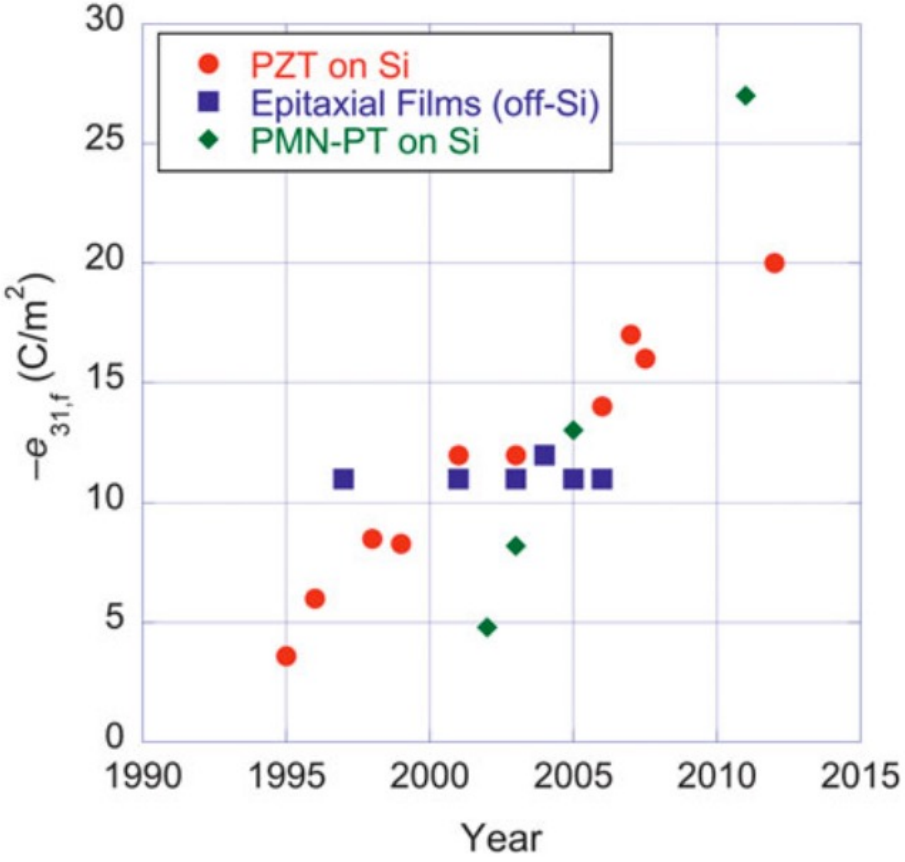

Figure 6. Evolution in piezoelectric $e_{31,f}$ coefficients, showing comparisons to data for bulk PZT materials. Data courtesy of P. Muralt. Adapted from Reference 45. Note: PZT, $Pb(Zr,Ti)O_3$; PMN-PT, $PbMg_{1/3}Nb_{2/3}O_3$–$PbTiO_3$.

C. Eom, S. Trolier-McKinstry, MRS BULLETIN VOLUME 37 NOVEMBER 2012 www.mrs.org/bulletin

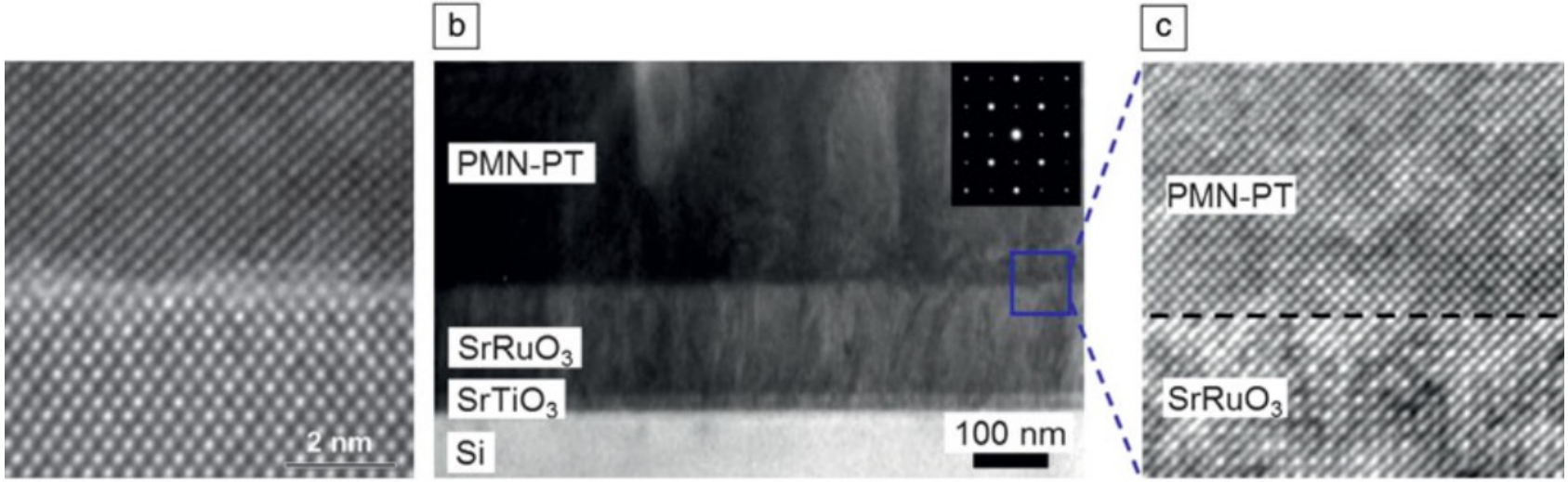

(a) High resolution transmission electron microscope (TEM) image of epitaxial $SrTiO_3$ on silicon grown by molecular beam
urtesy of Xiaoqing Pan of the University of Michigan and Darrell Schlom at Cornell University.) $SrRuO_3$ can then be epitaxi
top of the $SrTiO_3$ by off-axis sputtering to serve as the templating layer for the piezoelectrics, as well as a bottom electroc
field cross-sectional TEM image of an epitaxial $PbMg_{1/3}Nb_{2/3}O_3$–$PbTiO_3$ (PMN-PT)/$SrRuO_3$/$SrTiO_3$ thin-film heterostructure
te. The inset shows the selective area electron diffraction pattern of the PMN-PT layer along the [100] zone axis showing
) High-resolution TEM image of PMN-PT and $SrRuO_3$ interface. (b) and (c) are adapted from Reference 65.

C. Eom, S. Trolier-McKinstry, MRS BULLETIN VOLUME 37 NOVEMBER 2012 www.mrs.org/bulletin

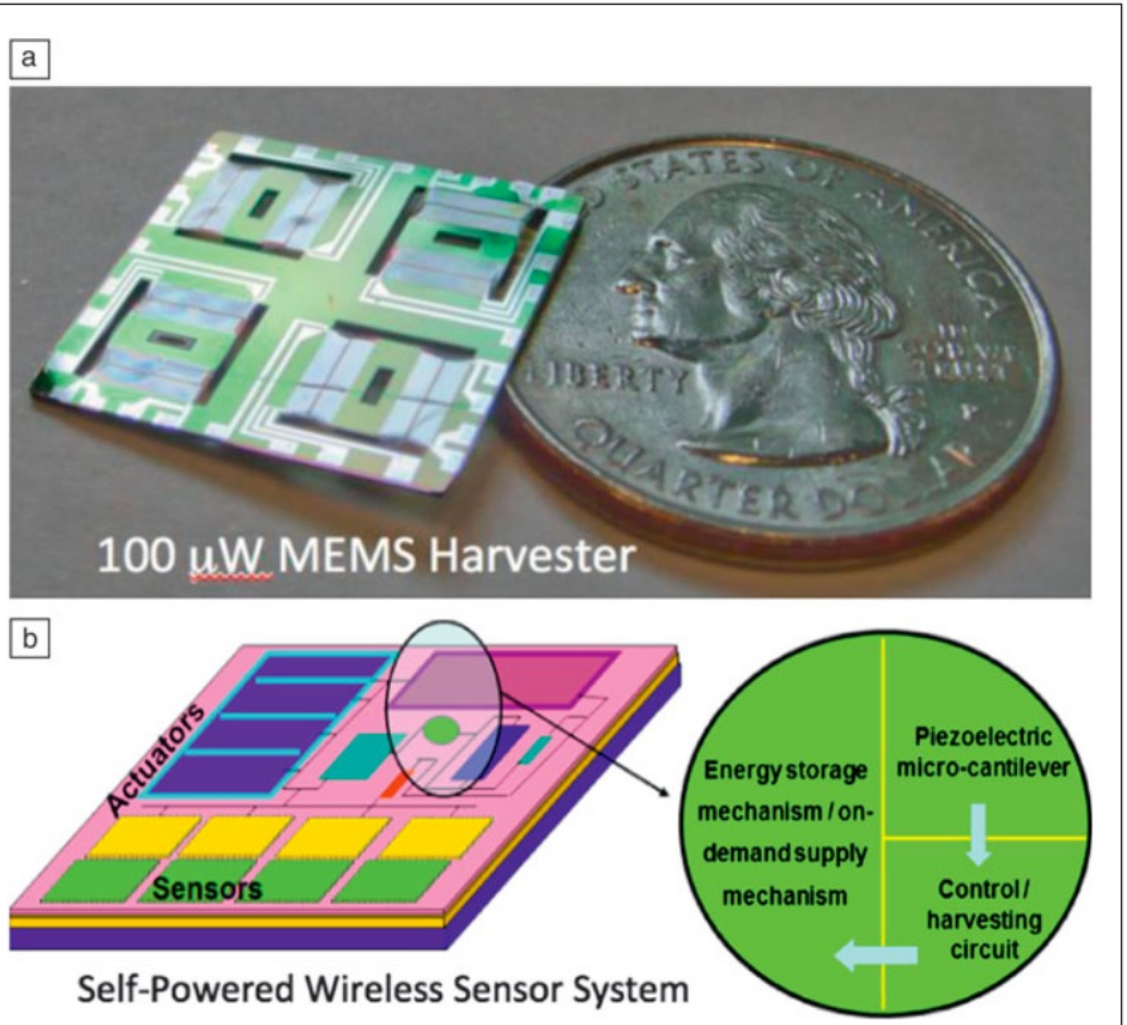

Figure 9. Examples of piezoelectric energy harvesting systems. (a) Photograph of a compact piezoelectric microelectromechanical system (MEMS) energy harvesting device, which is about the size of a US quarter ($0.25) coin. A doubly clamped beam acts as a frequency locked loop, resulting in wide bandwidth, non-linear resonance. (b) Schematic of on-chip architecture for a self-powered wireless sensor network system. Robust self-powering can be achieved by utilizing all environmental energy resources, as well as dual purpose sensors and actuators, which also act as energy harvesters.[87]

C. Eom, S. Trolier-McKinstry, MRS BULLETIN VOLUME 37 NOVEMBER 2012 www.mrs.org/bulletin

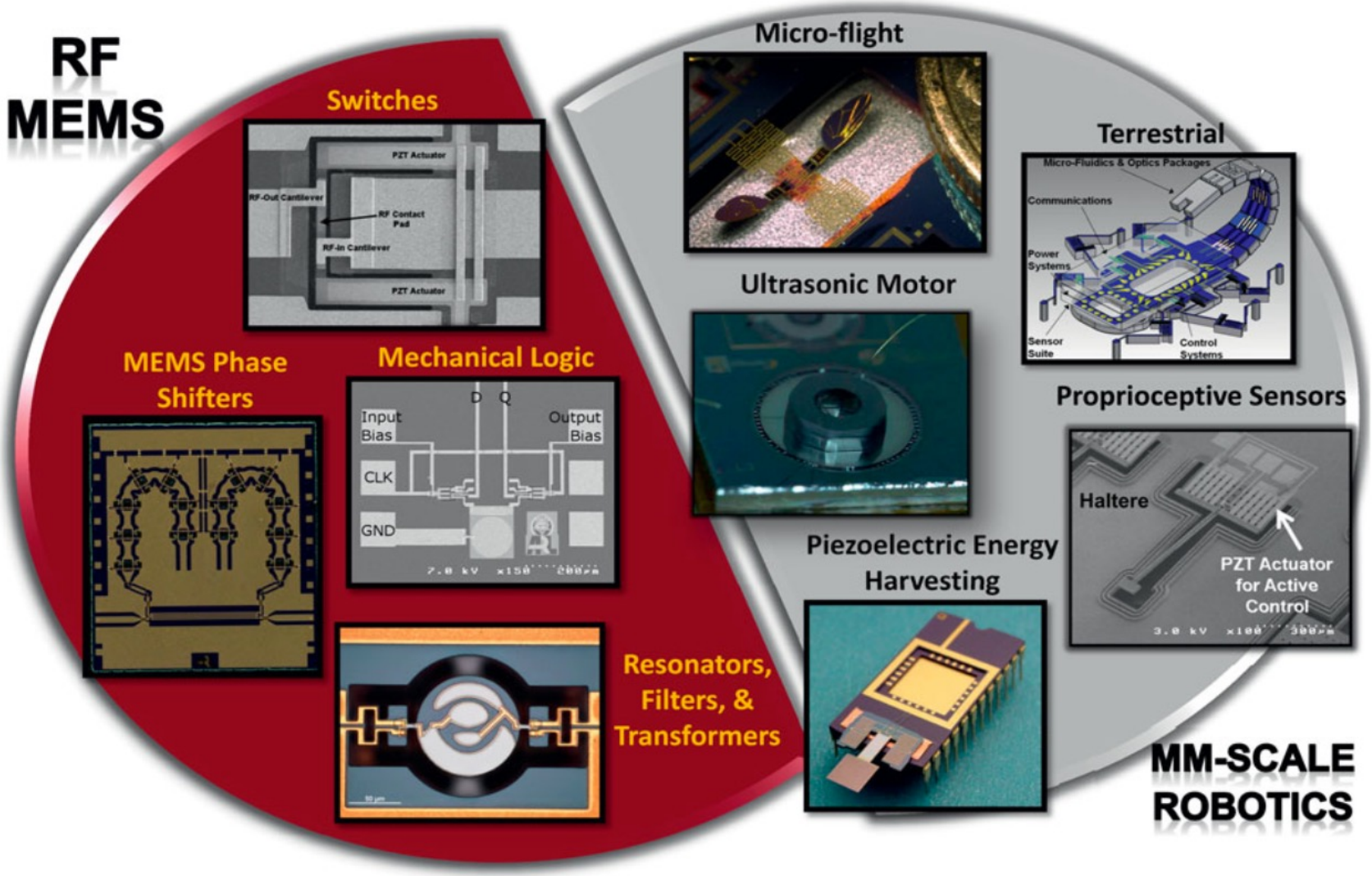

Figure 12. Montage of piezoelectric microelectromechanical (MEMS) devices. For the motor, the piezo MEMS stator is 3 mm in diameter, and the Si rotor is 2 mm in diameter. The switch uses a PZT actuator with a length of 125 microns. The phase shifter designed for 10 GHz operation has an overall dimension of 5.0 mm × 5.5 mm. The dual-wing micro wing structure was designed with 2 mm length wings. The piezoelectric energy harvester uses a 5-mm-long PZT thin-film cantilever that attached to a 5 mm × 5 mm proof mass. Image courtesy of Jeffrey S. Pulskamp and Ronald G. Polcawich, US Army Research Laboratory. Note: RF, radio frequency; PZT, $Pb(Zr,Ti)O_3$; CLK, clock; GND, ground.

Magnetron sputtering of ferroelectric thin film

- Target:
- Powder mixture, calcination in air 750C/3h, grounding + excess Bi2=3: Bi_2O_3,Nd_2O_3,Eu_2O_3,TiO_2
- Cu dish fillled with powder, pressed with 40 Mpa
- Deposition at 650 C on conductive rutiel Nb(0.8w%):TiO2 (101) substrate
- Sputter gas (Ar + ?) 0.1 – 5 Pa

M. Kobune et al, Japanese Journal of Applied Physics 54, 10NA01 (2015)

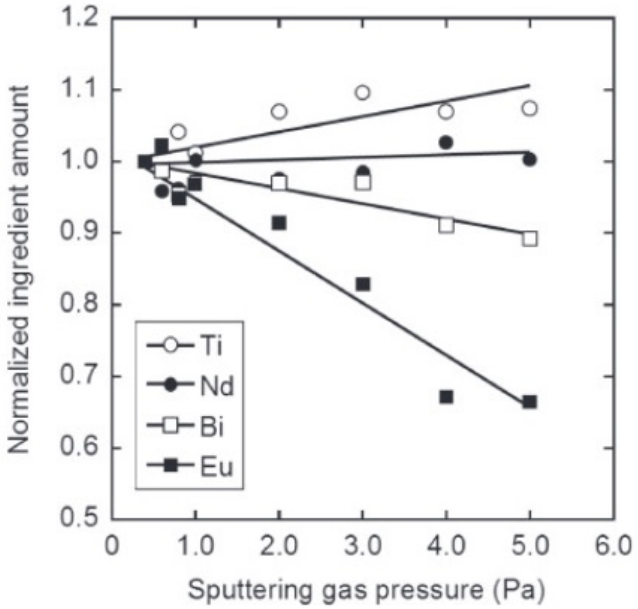

Fig. 3. Variation in film composition as a function of sputtering gas pressure. The Bi, Nd, Eu, and Ti contents were determined from the intensities of the Bi-Mα peak at 2.42 keV, the Nd-Lα peak at 5.23 keV, the Eu-Lα peak at 5.85 keV, and the Ti-Kα peak at 4.51 keV in the EDS spectra, respectively. All values are normalized by the value at 0.4 Pa for the corresponding element.

M. Kobune et al, Japanese Journal of Applied Physics 54, 10NA01 (2015)

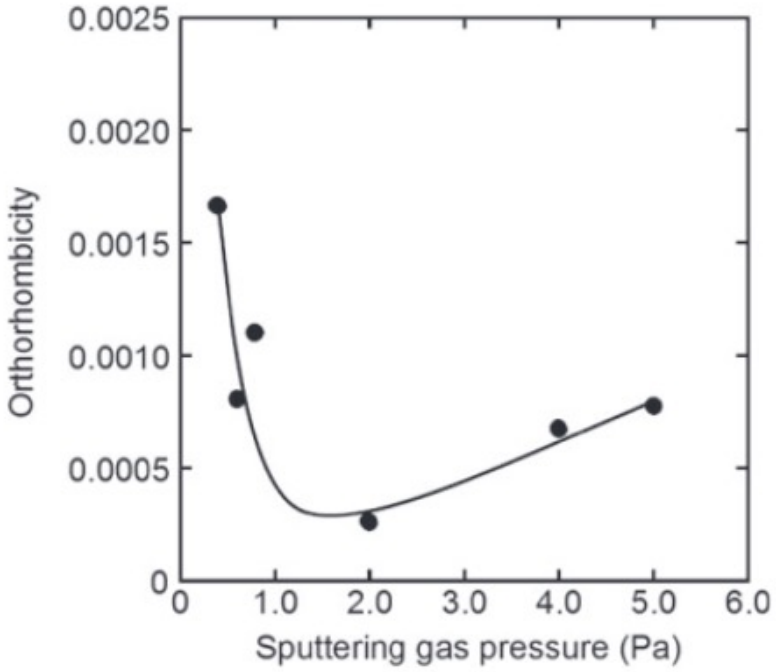

Fig. 4. Variation in room-temperature orthorhombicity of BNEuT-0.1 films as a function of sputtering gas pressure.

M. Kobune et al, Japanese Journal of Applied Physics 54, 10NA01 (2015)

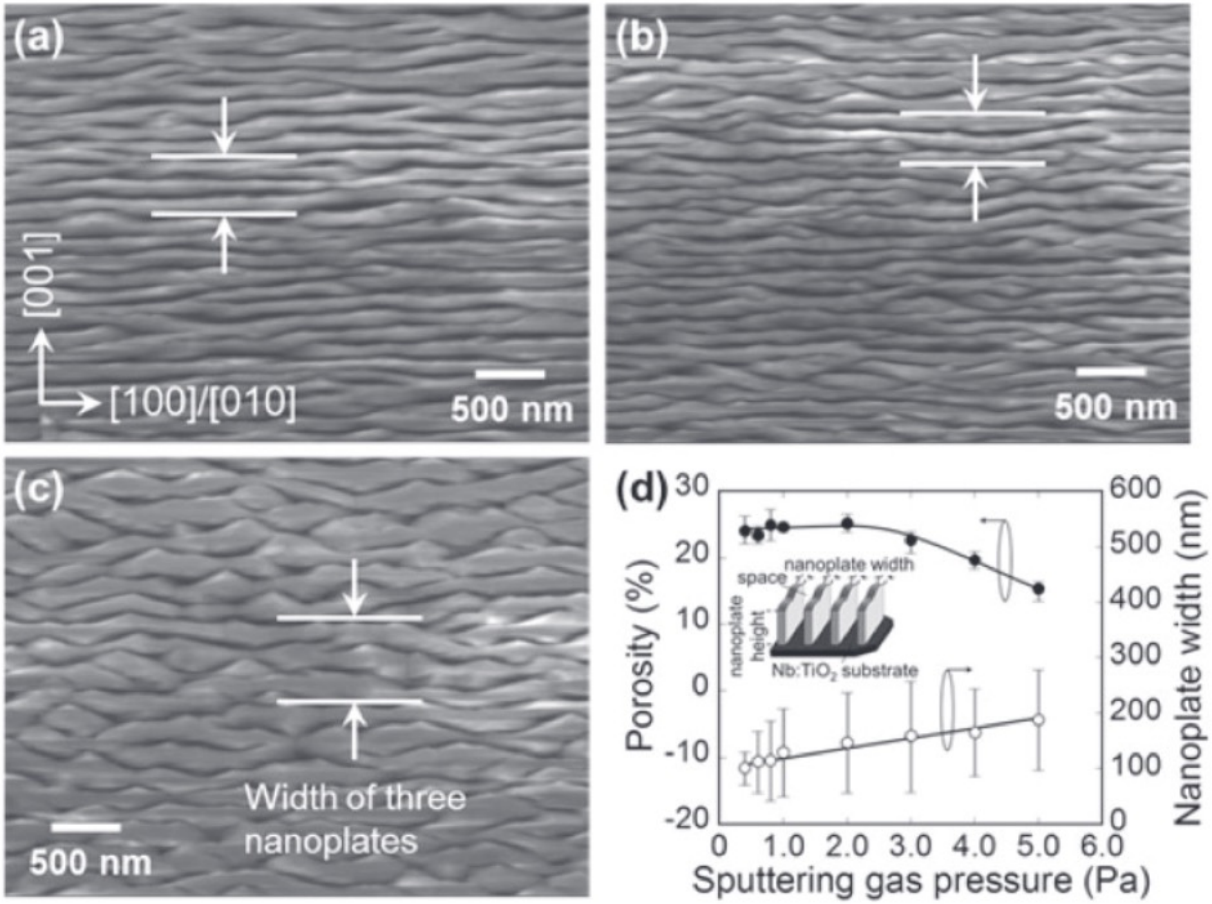

Fig. 5. Surface FE-SEM images of 1.8–2.3-μm-thick BNEuT-0.1 films deposited at (a) 0.4, (b) 1.0, and (c) 5.0 Pa, and (d) variation in nanoplate width along [001] direction as a function of sputtering gas pressure.

M. Kobune et al, Japanese Journal of Applied Physics 54, 10NA01 (2015)

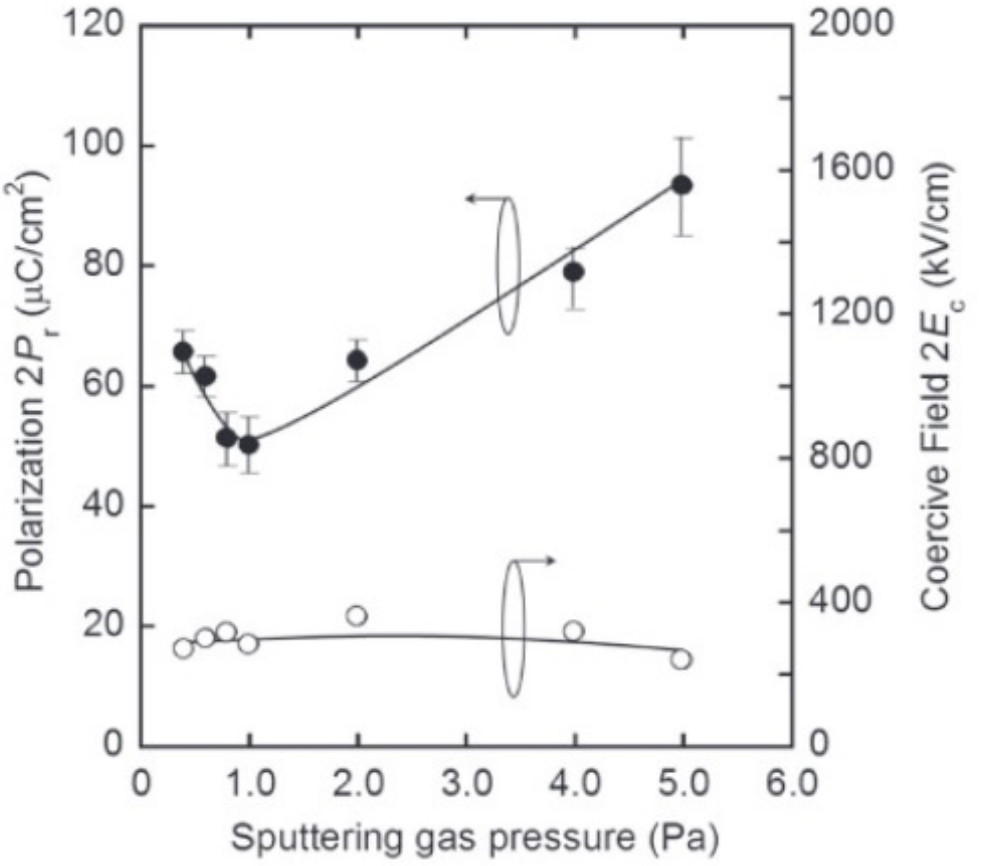

Fig. 7. Variations in room-temperature remanent polarization ($2P_r$) and coercive field ($2E_c$) for BNEuT-0.1 films with thicknesses of 1.8–2.3 μm as a function of sputtering gas pressure.

M. Kobune et al, Japanese Journal of Applied Physics 54, 10NA01 (2015)

Ultra thin film protection of hard disks

Magnetic rigid disc drive

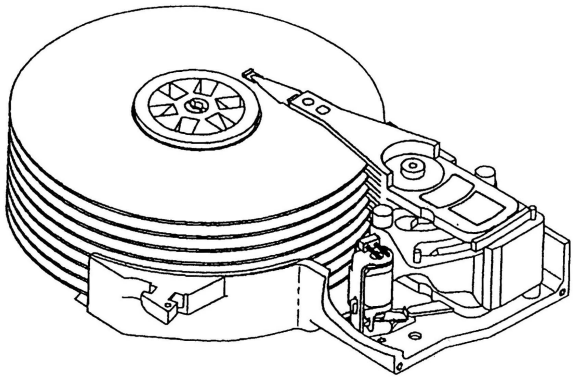

Magnetic rigid-disk drive

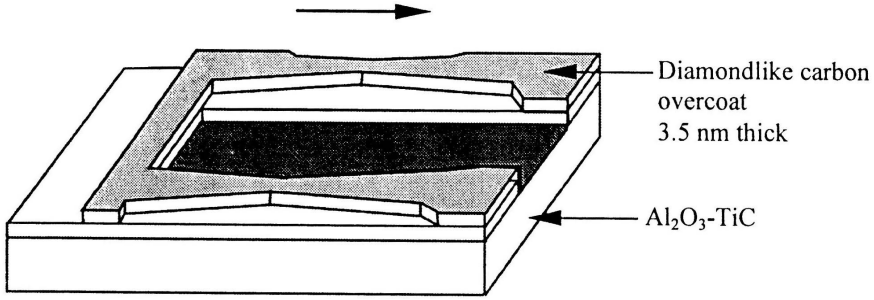

MR type picoslider

- A rigid disc drive consists of a stack of discs mounted on a spindle
- Disc stack is rotated at speed ranging from a few thousand to max. 15 000 rpm

  A head slider is supplied for each disc surface.

Source: Bhushan, B. 2001. Fundamentals of Tribology and Bridging the gap between the macro- and micro/Nanoscales. Kluwer Academic Publ.

Magnetic rigid disc drive

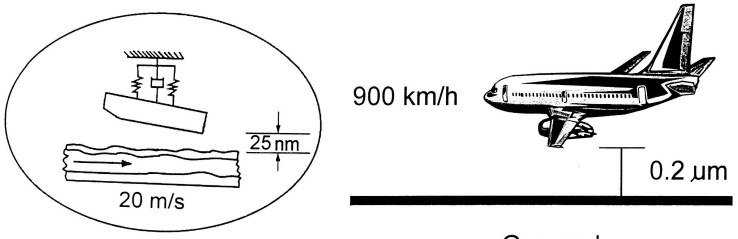

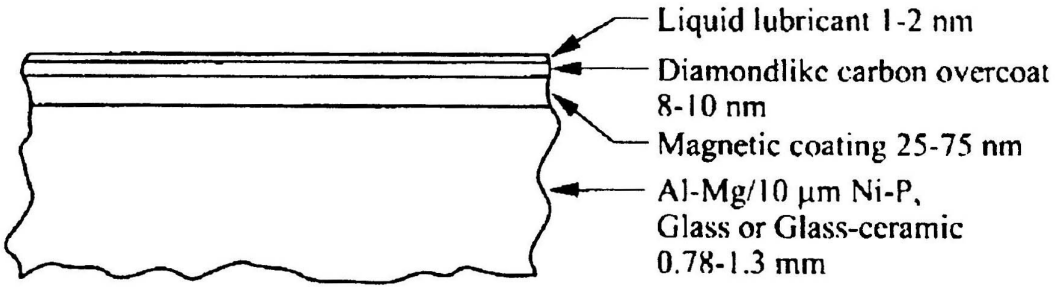

Thin-film disk

- **Increasing high recording densities requires smooth surfaces and low flying heights**
- **In modern rigid disc drives flying height ranges from 20 to 50 nm and surface roughness from 1.5 to 5 nm RMS.**

Source: Bhushan, B. 2001. Fundamentals of Tribology and Bridging the gap between the macro- and micro/Nanoscales. Kluwer Academic Publ.

Optical thin film stacks

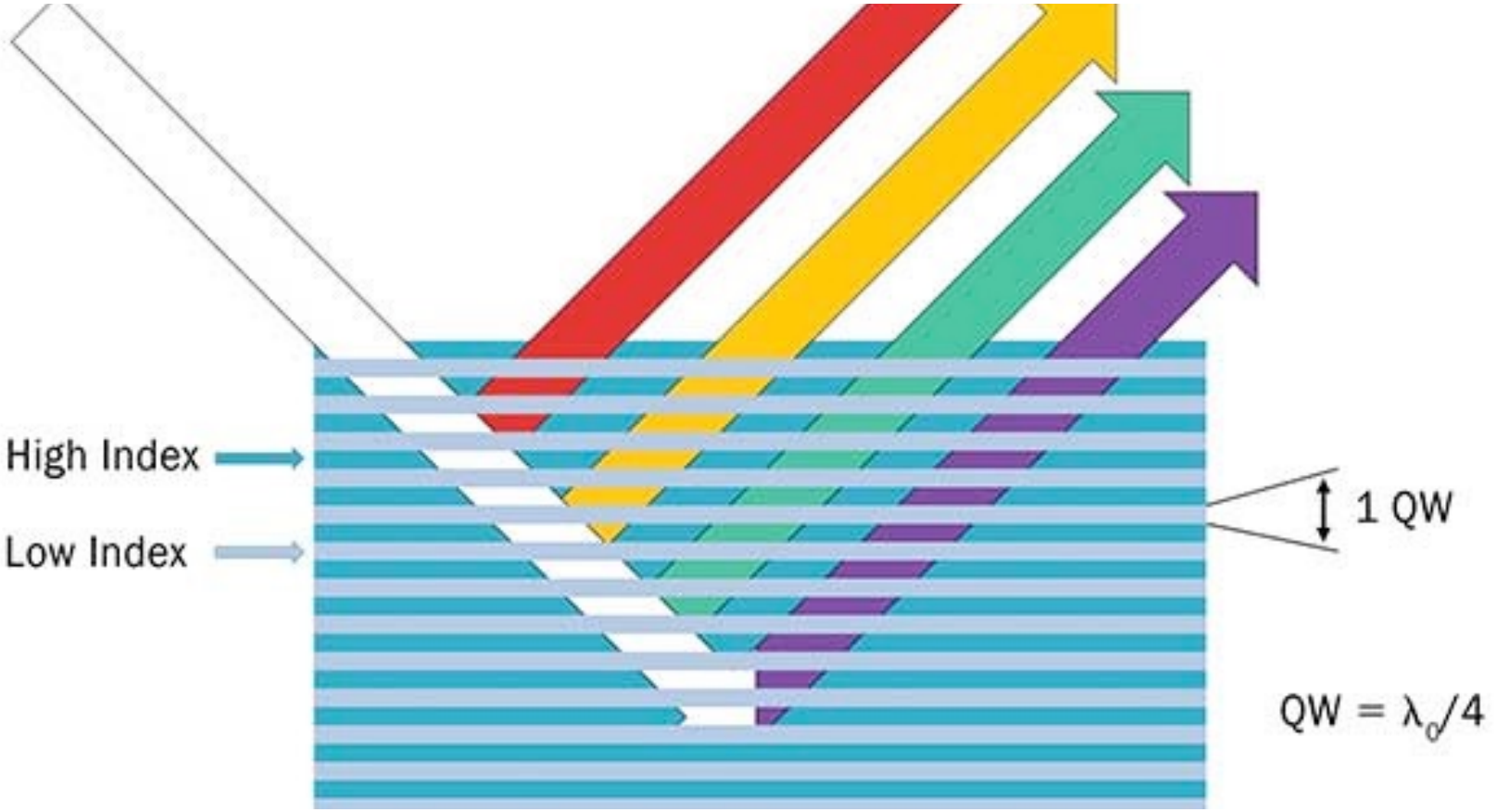

https://www.photonics.com/

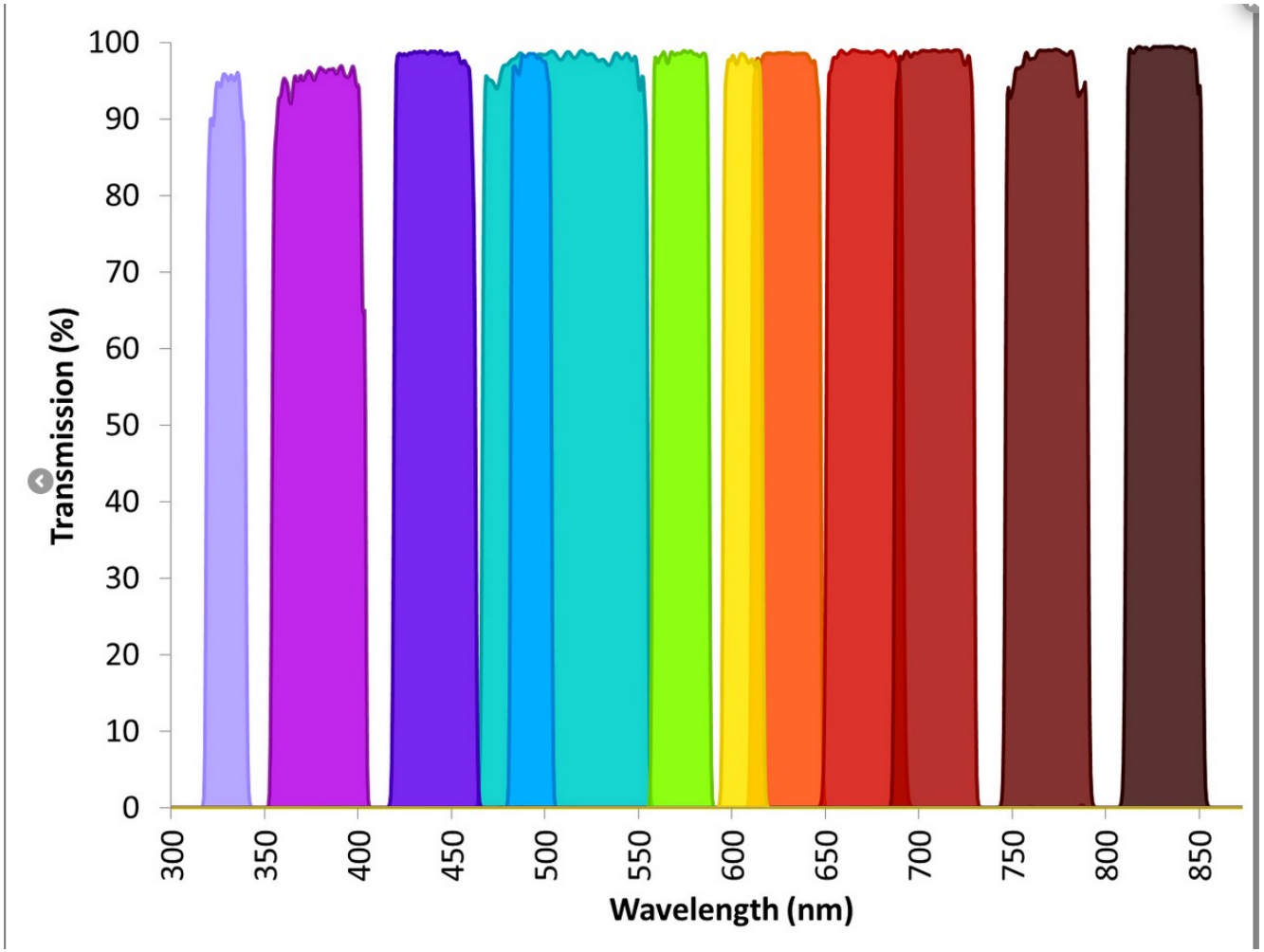

http://www.alluxa.com/learning-center/item/39-next-generation-thin-film-optical-filters-for-life-sciences

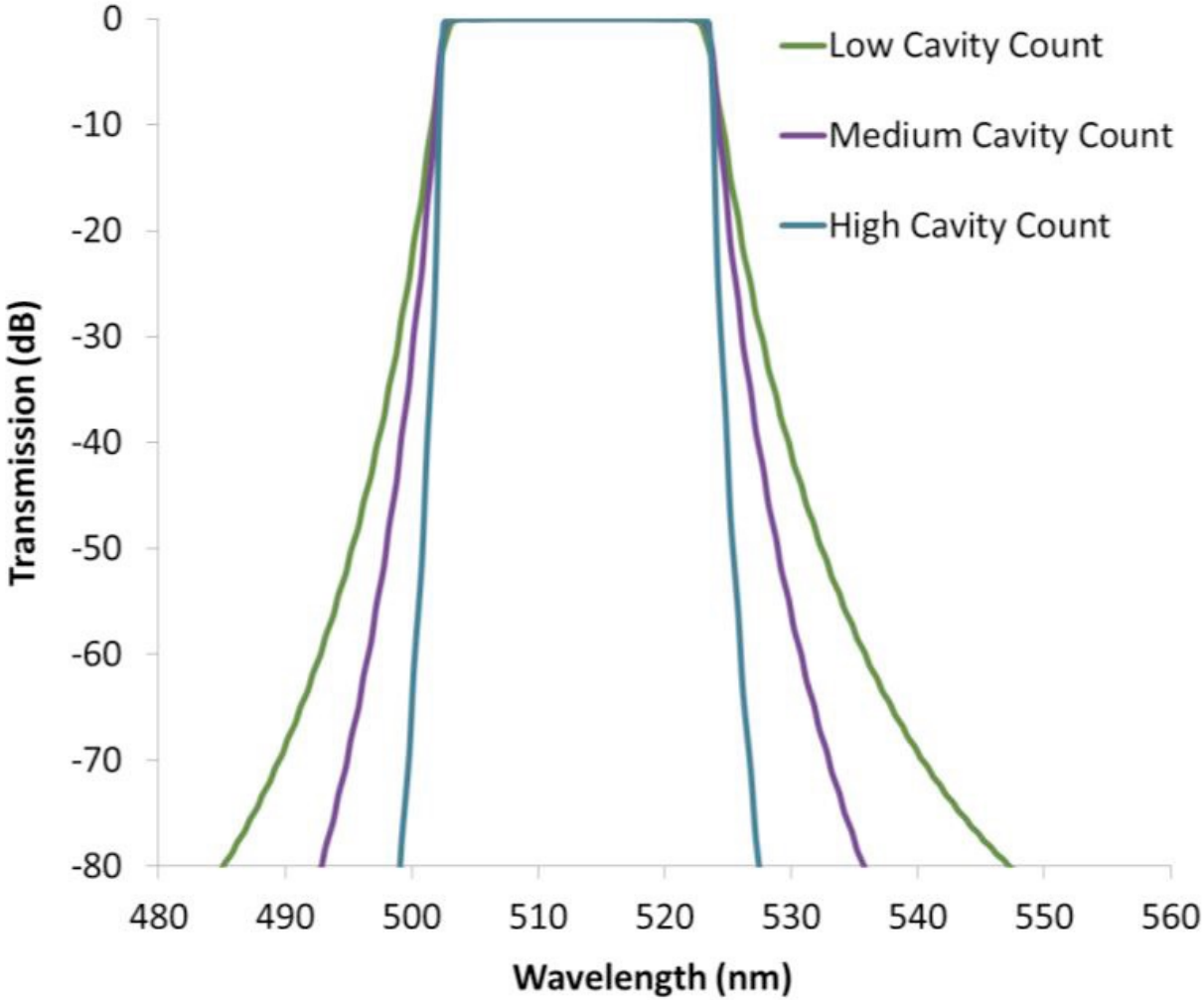

Figure 4. Filter "squareness" is a direct function of the number of resonant Fabry-Perot cavities in cavity filters, or the number of layers in LWP / SWP designs.

http://www.alluxa.com/learning-center/item/39-next-generation-thin-film-optical-filters-for-life-sciences

Deposition

- Evaporation
- Magnetron sputtering
- Ionbeam sputtering
- ALD

TABLE 2.

TYPICAL OPTICAL COATING MATERIALS CATEGORIZED BY SPECTRAL REGION AND REFRACTIVE INDEX INCLUDE PURE FORMULATIONS AND NOT MIXTURES

Wavelength Region (nm)	Low Index n < 1.6	Intermediate n 1.6 - 1.8	High Index n ~2
UV: 250 - 400	MgF_2, SiO_2, CeF_3	Al_2O_3, Y_2O_3	HfO_2, Sc_2O_3
Visible - NIR: 400 - 1100	SiO_2, MgF_2	Al_2O_3, Y_2O_3	Ta_2O_5, Nb_2O_5, $LaTiO_3$, TiO_2
UV: 250 - 400	MgF_2, SiO_2, CeF_3	Al_2O_3, Y_2O_3	HfO_2, Sc_2O_3
SW - MWIR: 1100 - 5000	SiO_2, CeF_3	Al_2O_3, Y_2O_3, SiO	Ta_2O_5, $LaTio_3$, HfO_2
LWIR: 5000 - 12,000	CeF_3, YF_3, ThF_4	--	ZnS, ZnSe, Ge

Gas sensing

Ph.D. Thesis

Thin films for gas sensors

José Miguel Alves Correia Pires*

27/11/2003

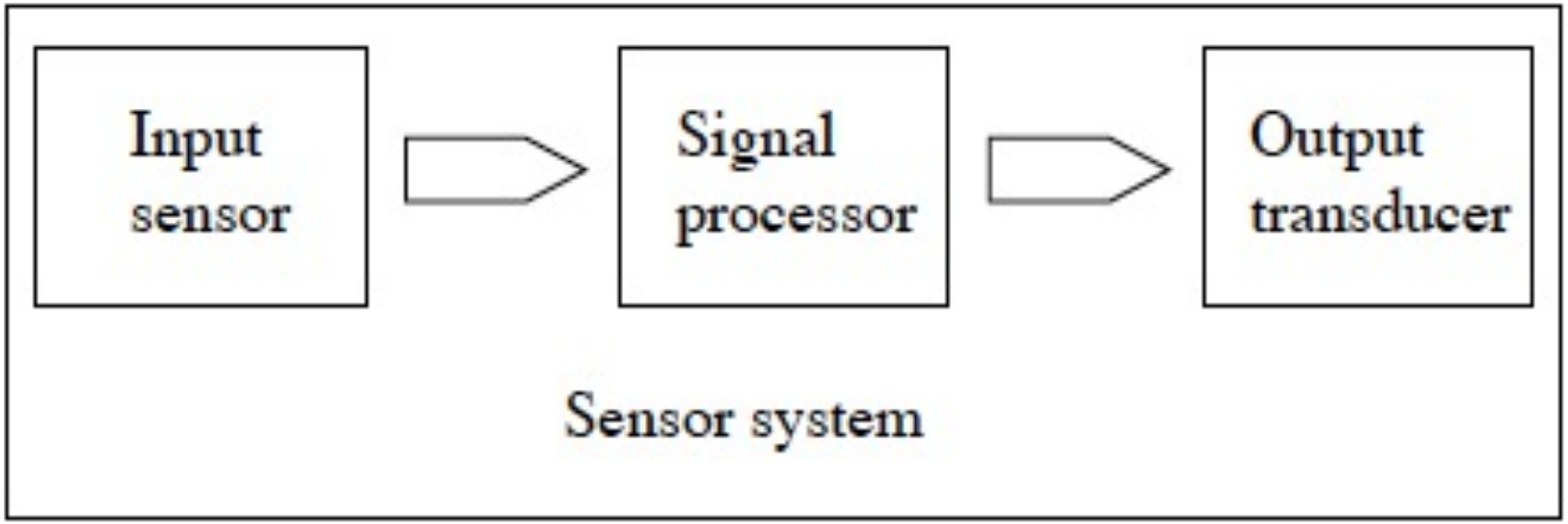

Figure 2.1.: Typical structure of a sensor system

Table 2.1.: Classification scheme based on the sensor' input stimulus

Class	Detected Properties
Mechanical	length, acceleration, flow, force, pressure, etc.
Thermal	temperature, specific heat, heat flow, etc.
Electrical	charge, current, voltage, resistance, inductance, etc.
Magnetic	magnetic flux density, magnetic moment, etc.
Optical	light intensity, wavelength, polarization, etc.
Radiation	type, number or energy of radiation particles; light properties far from the visible spectrum; etc.
Chemical	composition, concentration, pH, etc.

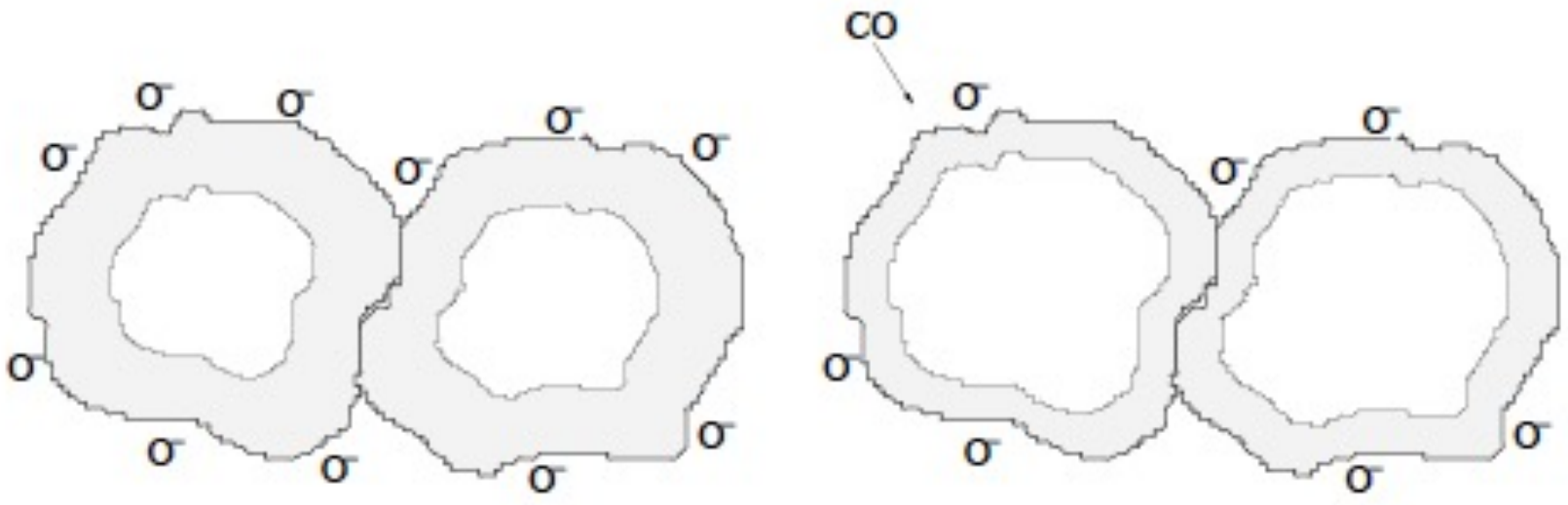

Figure 6.8.: Grain contact model and barrier control scheme

Table 4.1.: Range of parameters selected for DC and RF sputtering deposition of tin oxide samples

Parameter	DC sputtering	RF sputtering
Temperature (° C)	60–400	40–400
Source power (W)	—	200–800
Source current (A)	0.08–0.30	—
Pressure ($\times 10^{-1}$ Pa)	.25–12	4–10
O_2 flow rate (sccm)	3.6–14.8	25–50
Substrate-target distance (mm)	55–76	60–80
Sputtering time (min)	5–120	5–120
Pre-sputtering time (min)	2–27	0–10
Etching power (W)	—	100, 200
Etching time (min)	—	0, 10
Power applied to substrate bias (W)	—	0–50

Table 4.2.: Non-independent parameters controlled during deposition

Parameter	DC sputtering	RF sputtering
Target voltage (V)	200–350	—
Ar flow rate (sccm)	5.4–26	67–160
O_2 partial pressure ($\times 10^{-1}$ Pa)	.13–.65	4–10

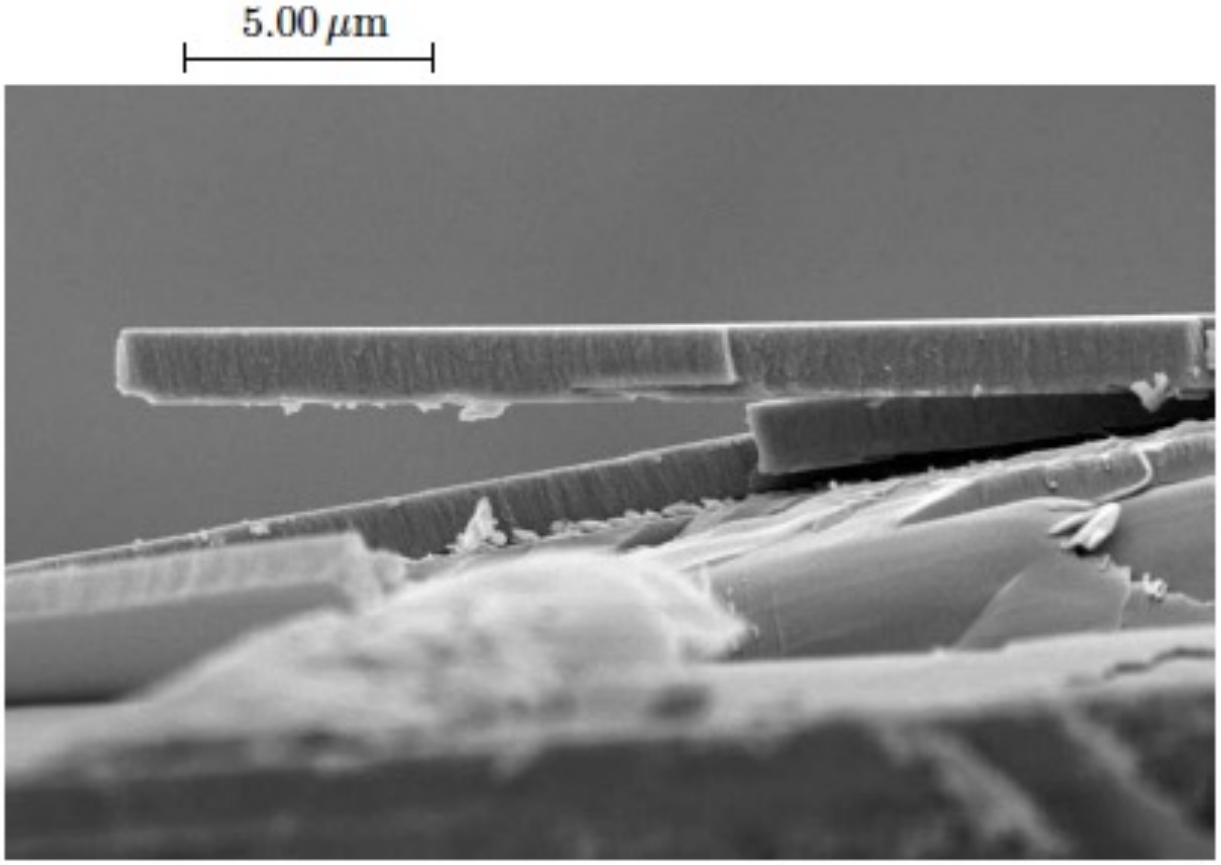

Figure 4.6.: SEM image showing delamination of a SnO_2 layer

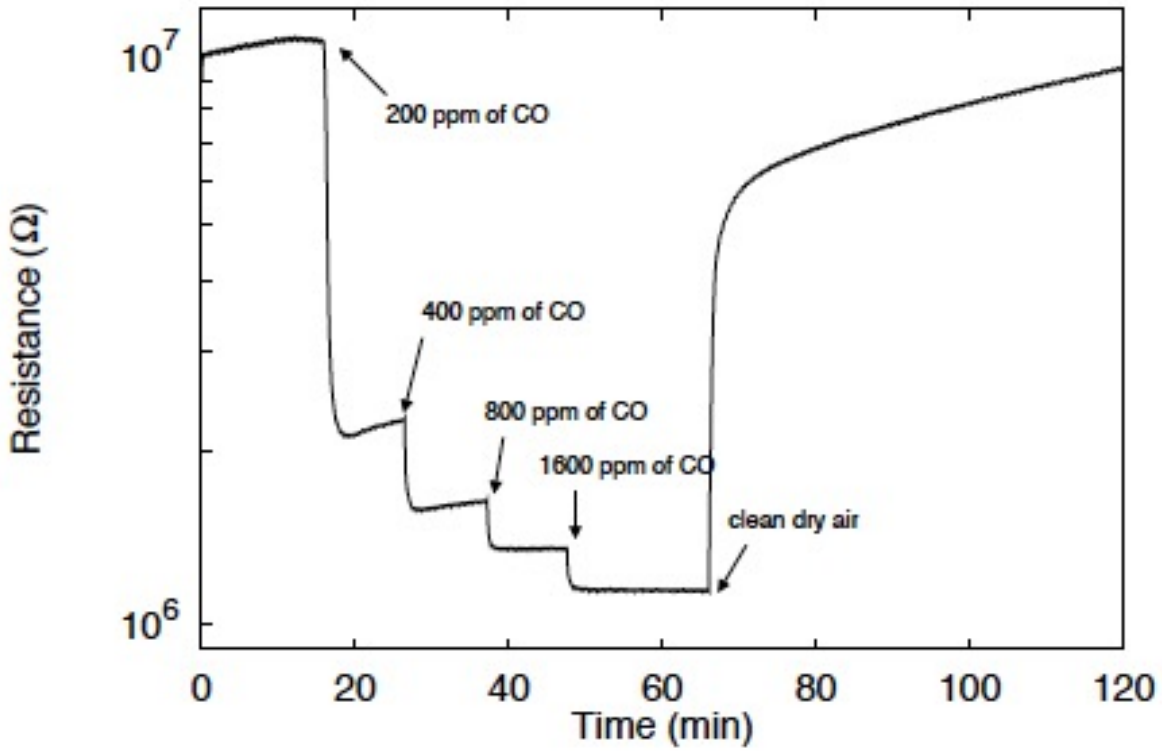

Figure 6.17.: Sample response to concentrations of carbon monoxide between 100 ppm and

Bio molecular sensing

3 Electrode electrochemical measurement: Ferrocyanide reduction

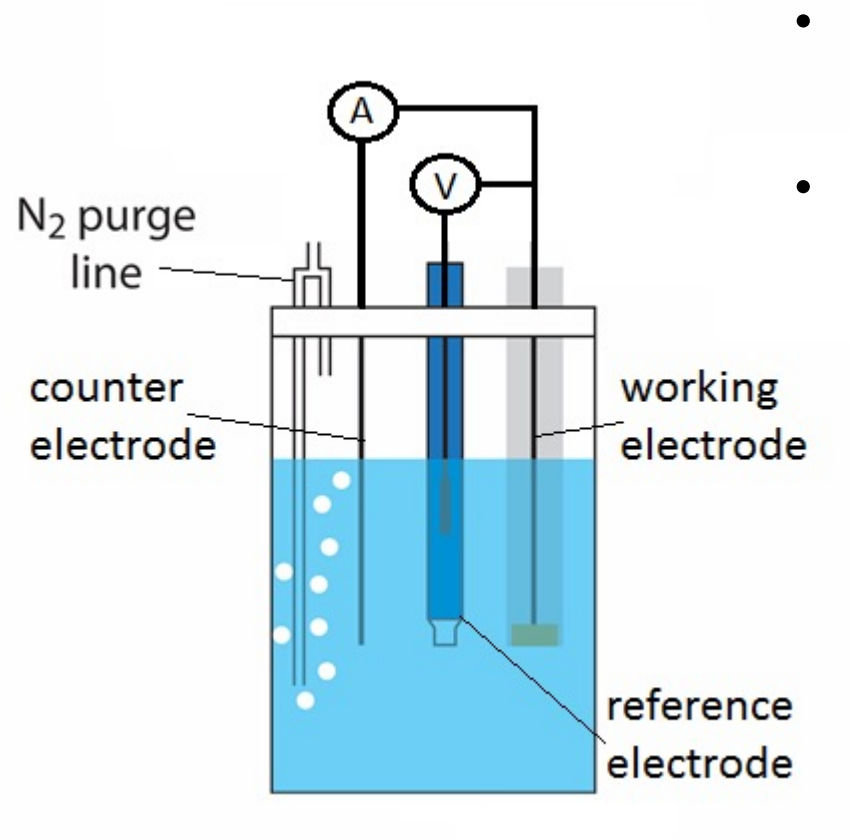

chem.libretexts.org/Textbook_Maps/Analytical_Chemistry_Textbook_Maps/Map%3A_Analytical_Chemistry_2.0_(Harvey)/11_Electrochemical_Methods/11.4%3A_Voltammetric_Methods

- Potential: between working and reference electrode
- Current measured between working and counter electrode

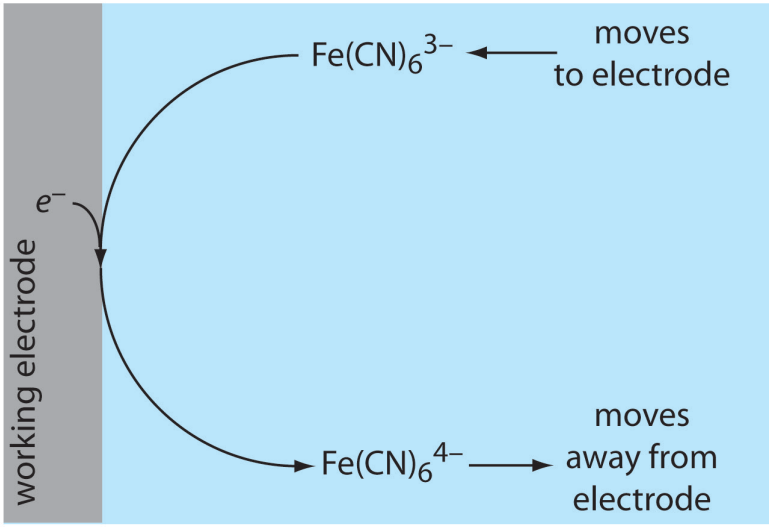

chem.libretexts.org/@api/deki/files/12486/Figure11.39.jpg?revision=1

Integrated thin film 3-electrode test strip

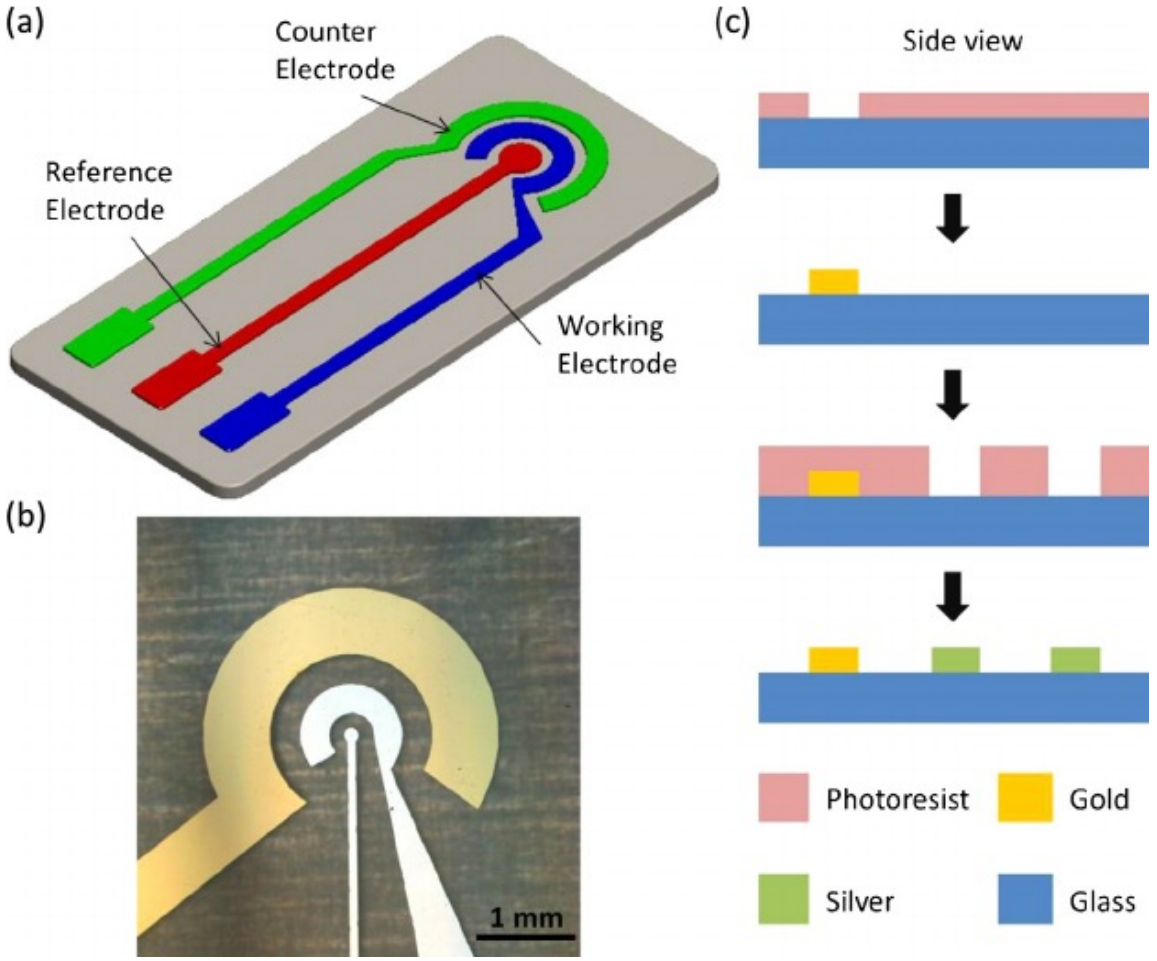

Xinhao Wang, Manas Ranjan Gartia, Jing Jiang, Te-Wei Chang, Junle Qian, Yong Liu, Xiangrong Liu, Gang Logan Liu, Audio jack based miniaturized mobile phone electrochemical sensing platform, Sensors and Actuators B: Chemical, Volume 209, 31 March 2015, Pages 677-685, ISSN 0925-4005

Electrochemical detection of Dopamine (DA)

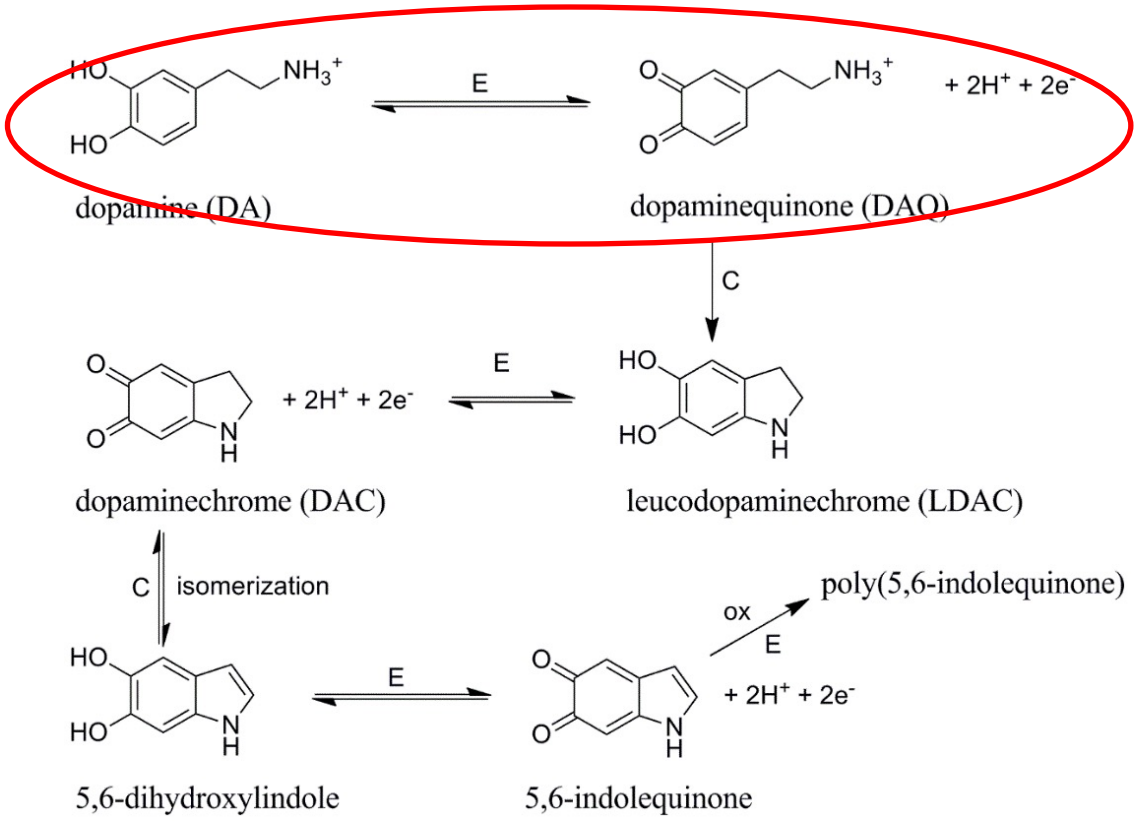

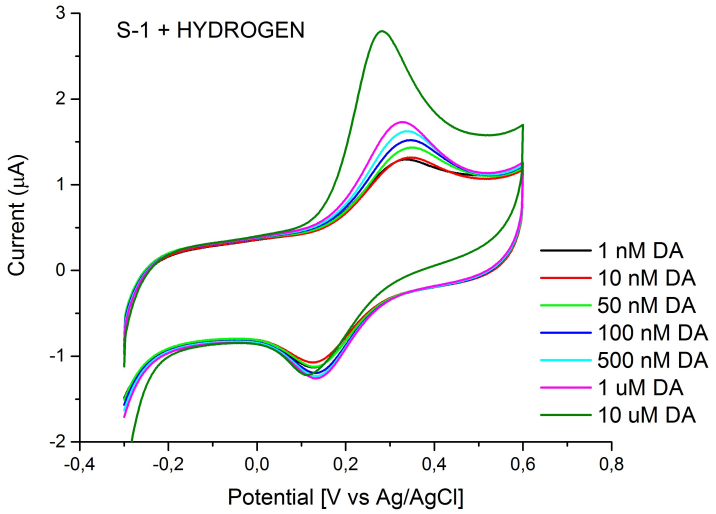

Detection of Morphine and codeine

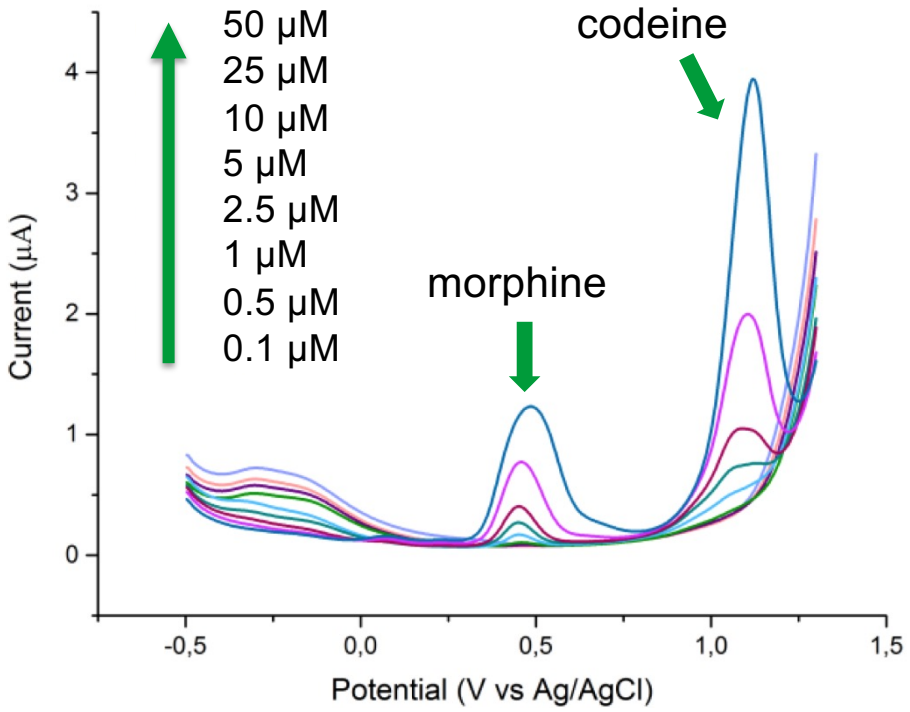

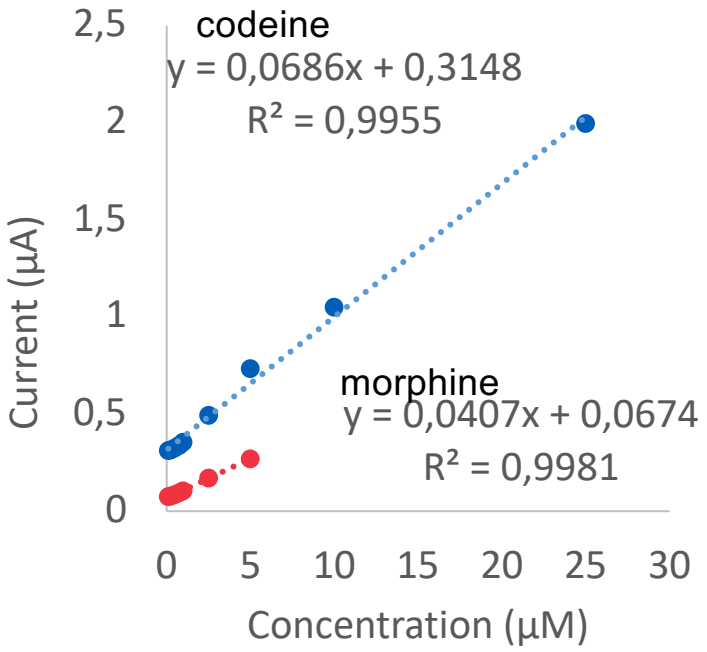

CNF for enzymatic detection of Glutamate

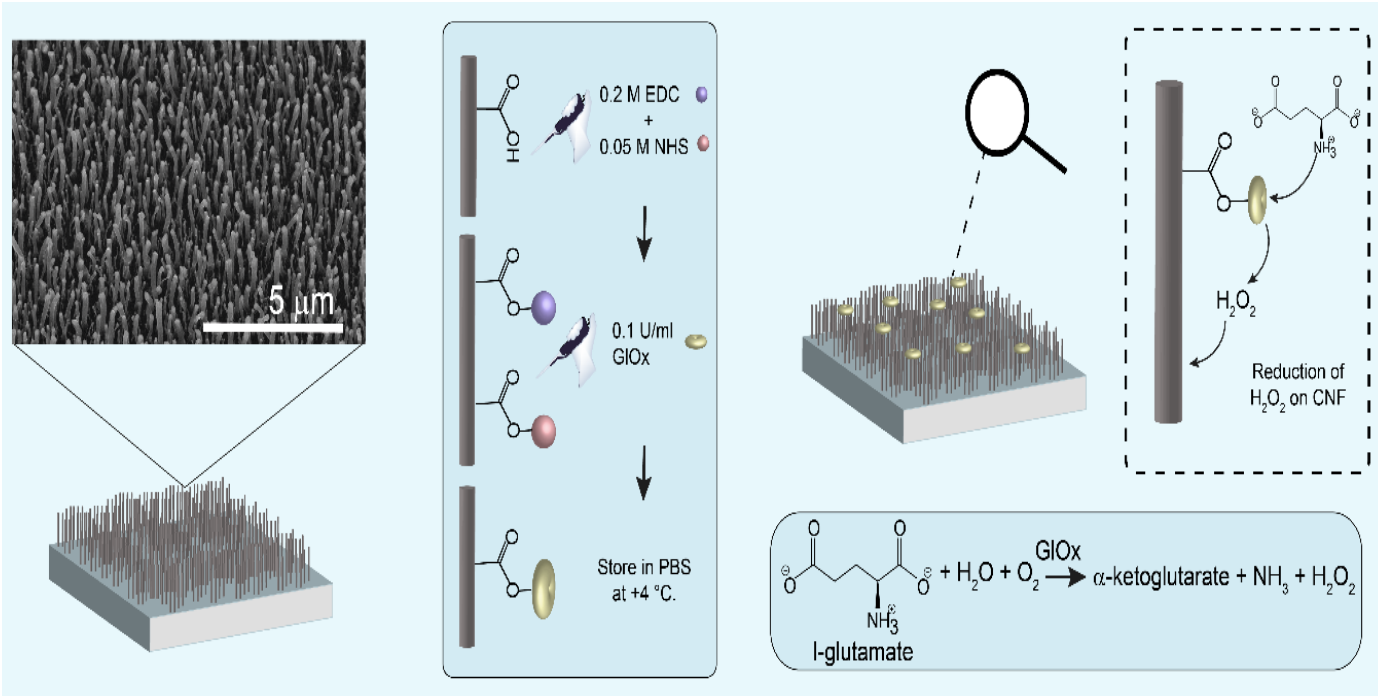

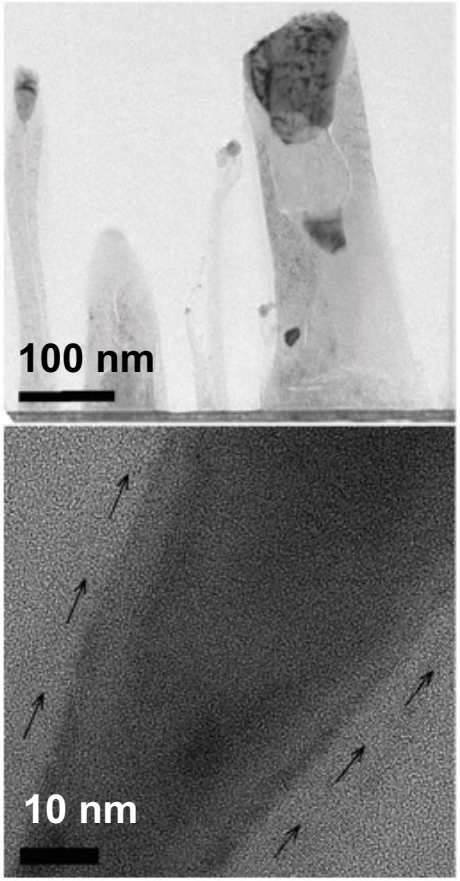

Isoaho, Noora, et al. "Carbon Nanostructure Based Platform for Enzymatic Glutamate Biosensors. " *The Journal of Physical Chemistry C* (2017).

CNF for enzymatic detection of Glutamate

Detection of H_2O_2, Reaction product of enzymatic oxidation

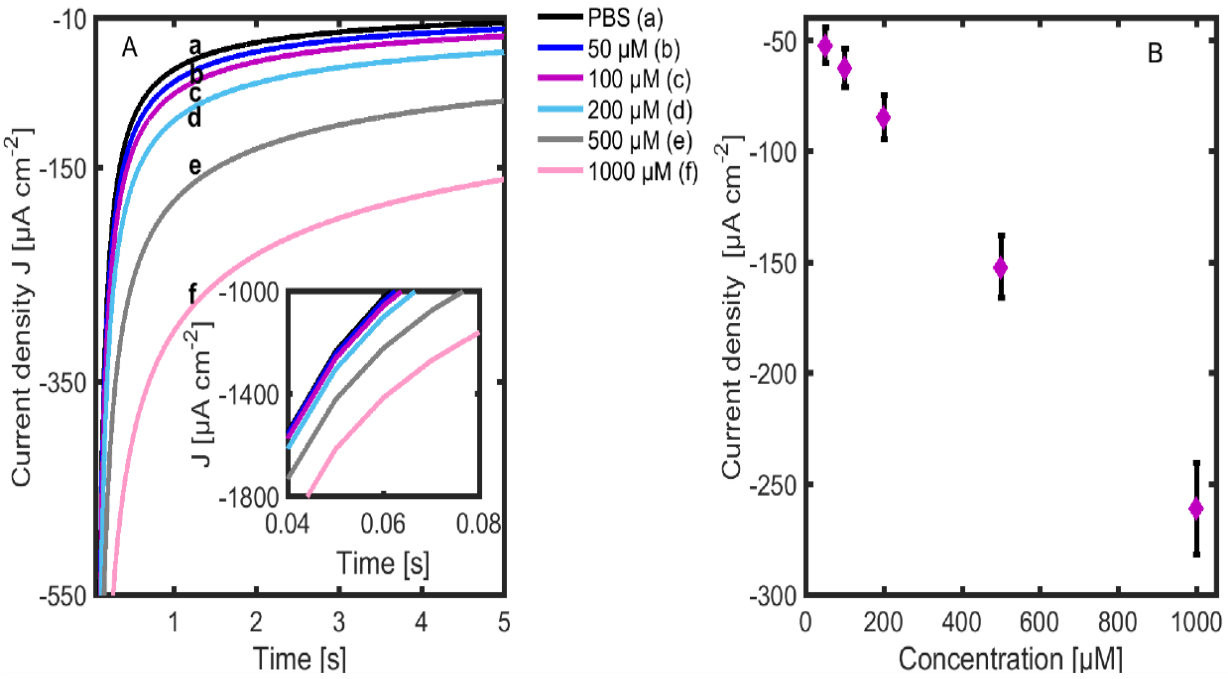

Isoaho, Noora, et al. "Carbon Nanostructure Based Platform for Enzymatic Glutamate Biosensors." *The Journal of Physical Chemistry C* (2017).

Pt-CNF for enzymatic detection of Glutamate

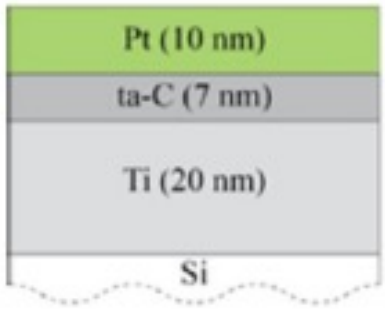

PECVD
With
$NH_3 + C_2H_2$

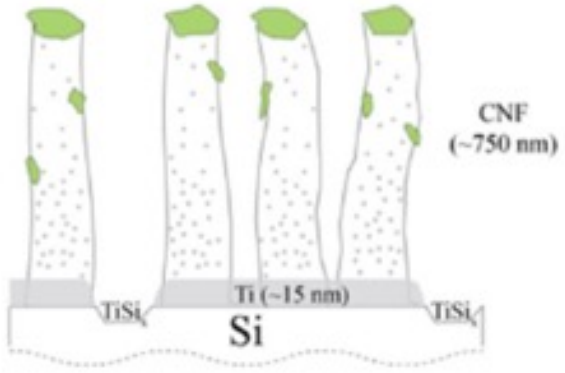

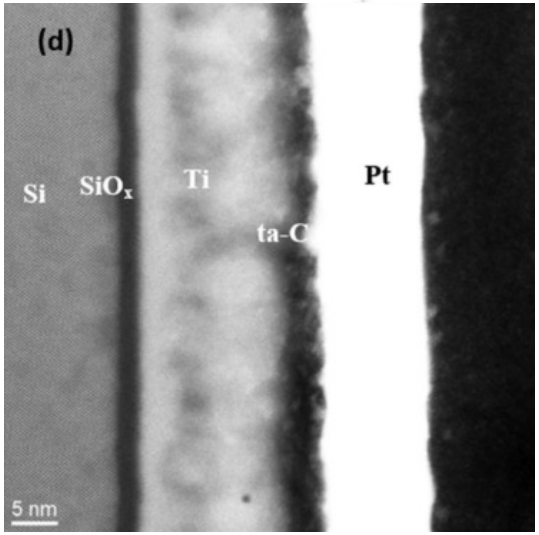

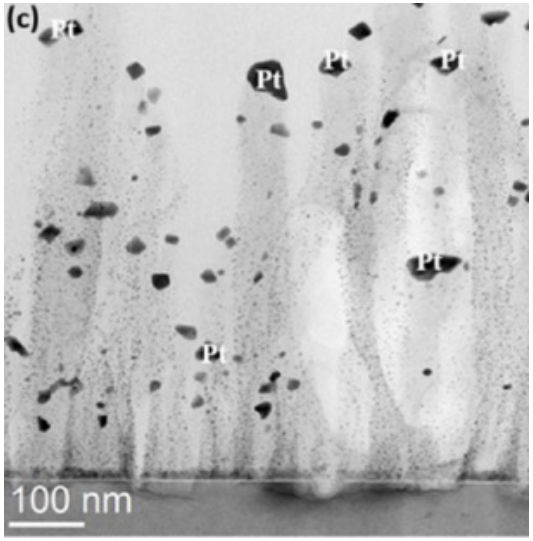

Laurila, Tomi, et al. "Application-Specific Catalyst Layers: Pt-Containing Carbon Nanofibers for Hydrogen Peroxide Detection." *ACS Omega* 2.2 (2017): 496-507.

Pt-CNF for enzymatic detection of Glutamate

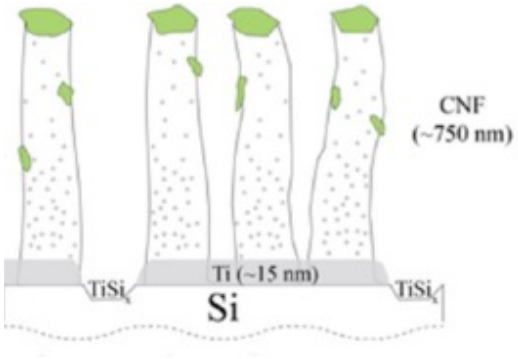

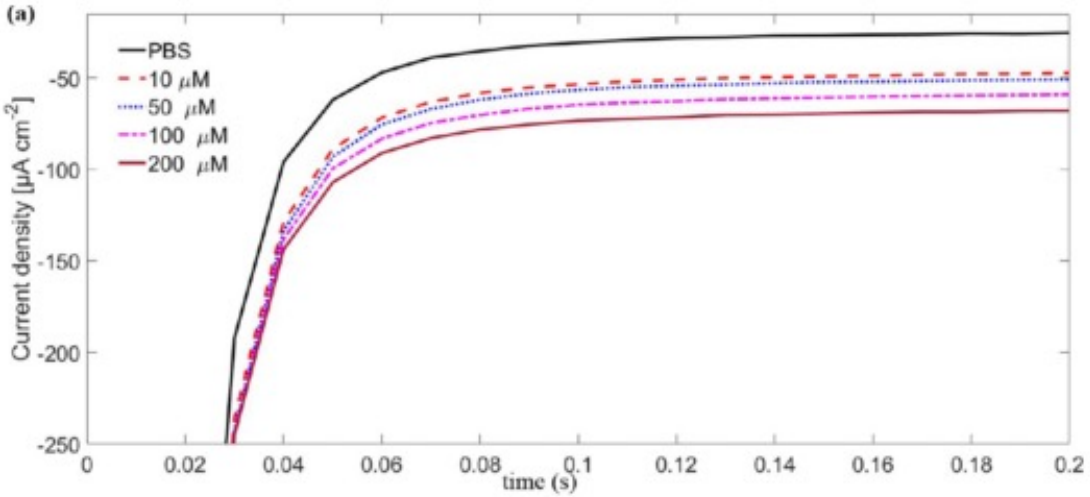

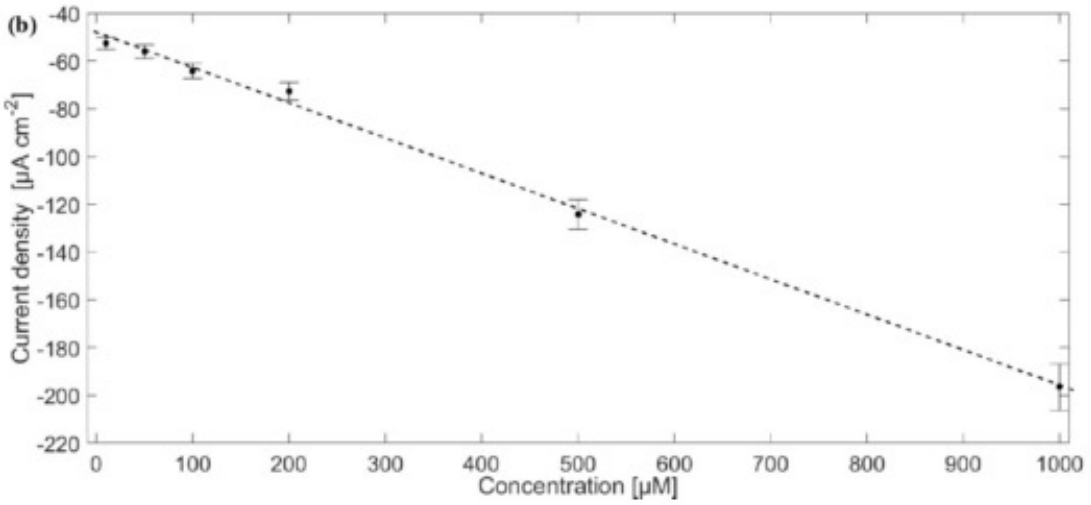

Photocatalytic TiO2 films

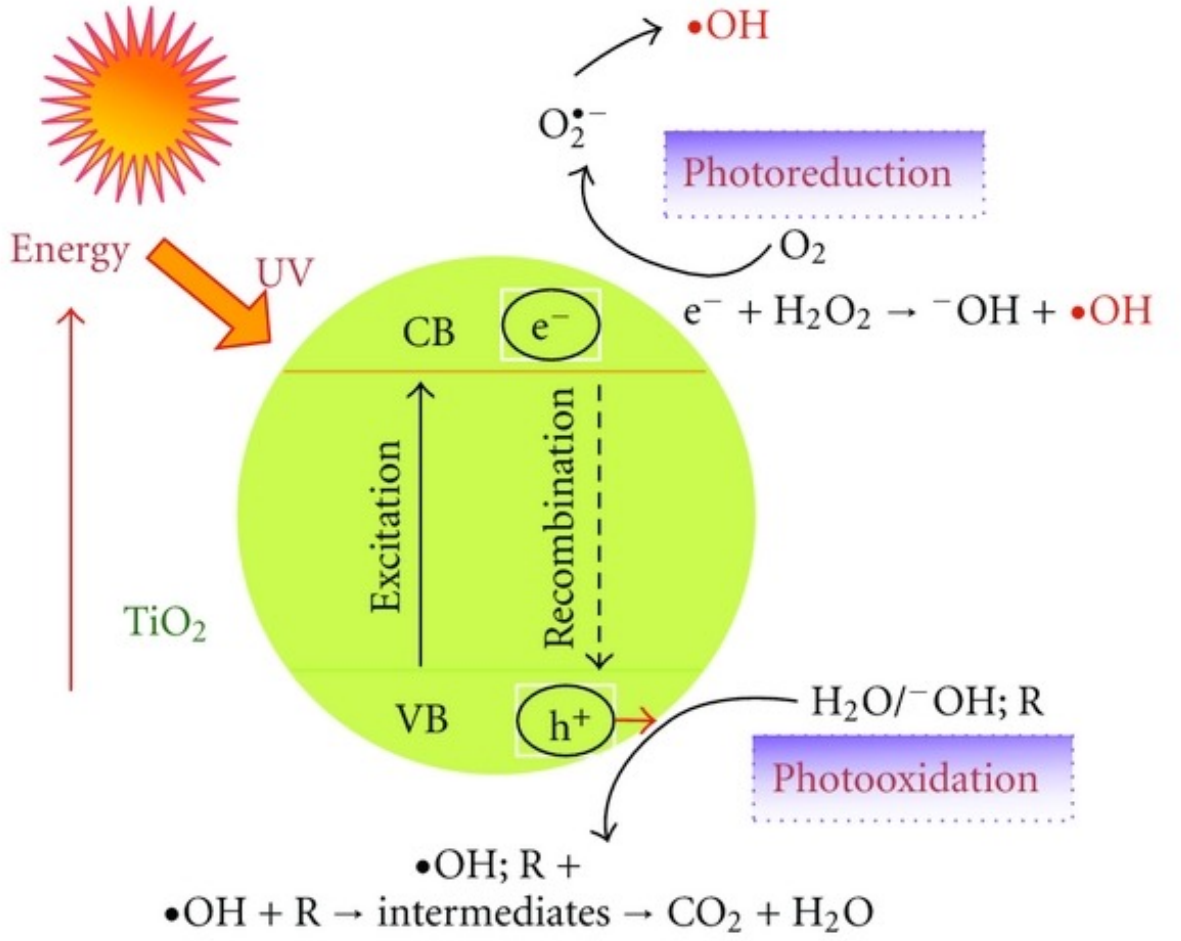

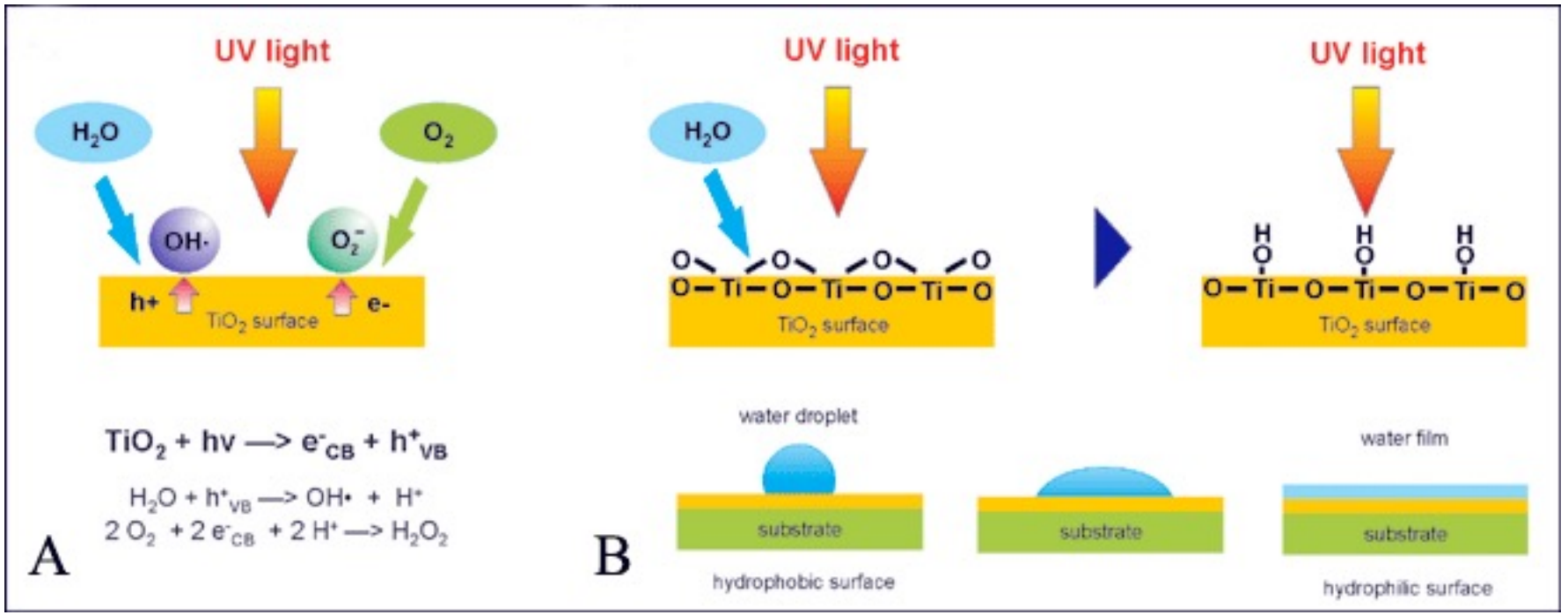
UV light
H2O
O2
OH·
O2−
h+
TiO2 surface
e-
TiO2 + hv —> e-CB + h+VB
H2O + h+VB —> OH• + H+
2 O2 + 2 e-CB + 2 H+ —> H2O2
A
UV light
H2O
O Ti O Ti O Ti O
TiO2 surface
UV light
H O
O Ti O Ti O Ti O
TiO2 surface
B
water droplet
substrate
hydrophobic surface
substrate
water film
substrate
hydrophilic surface

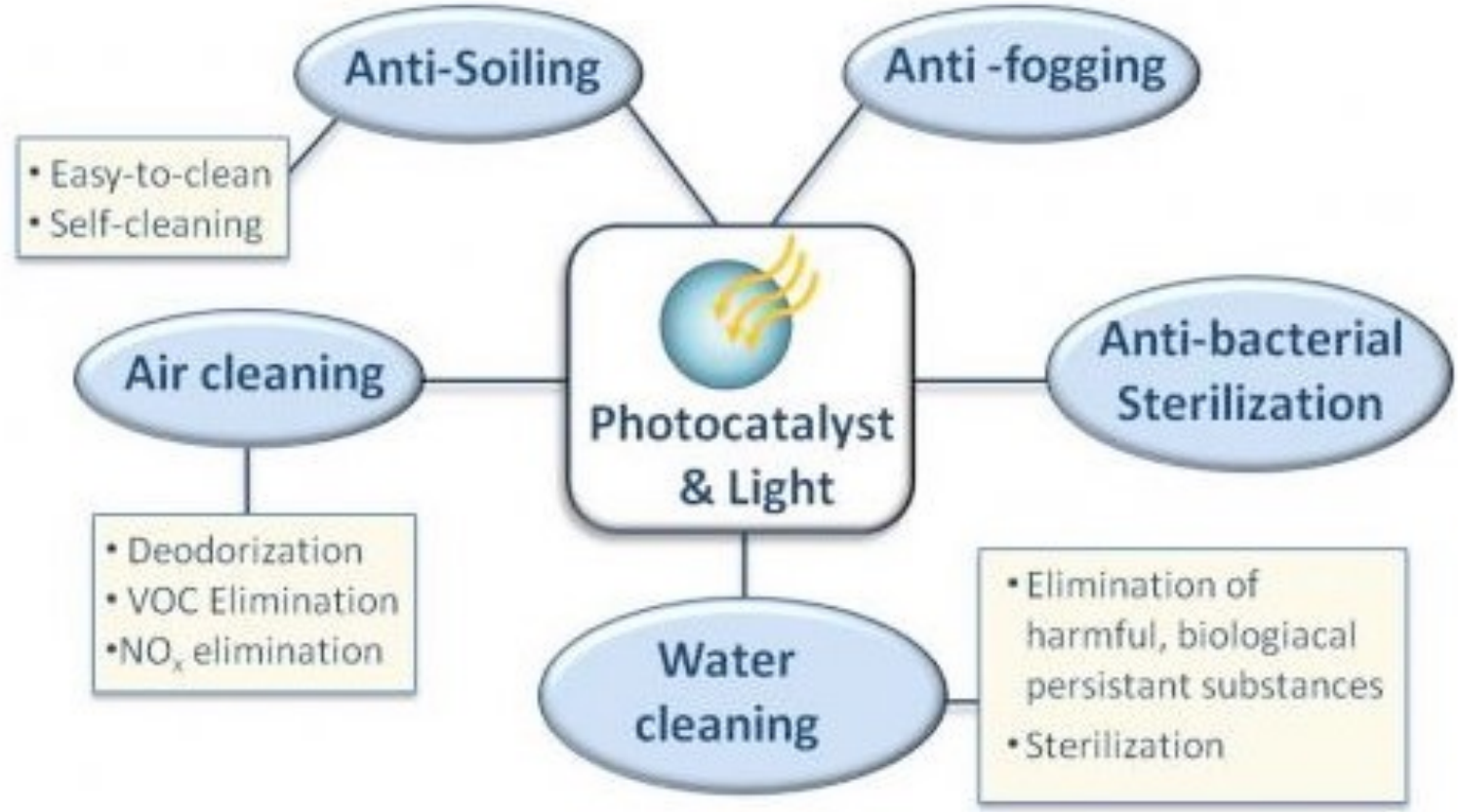

http://vdmi.de/englisch/products/applied-photocatalysis.html

http://www.teknik.uu.se/solid-state-physics

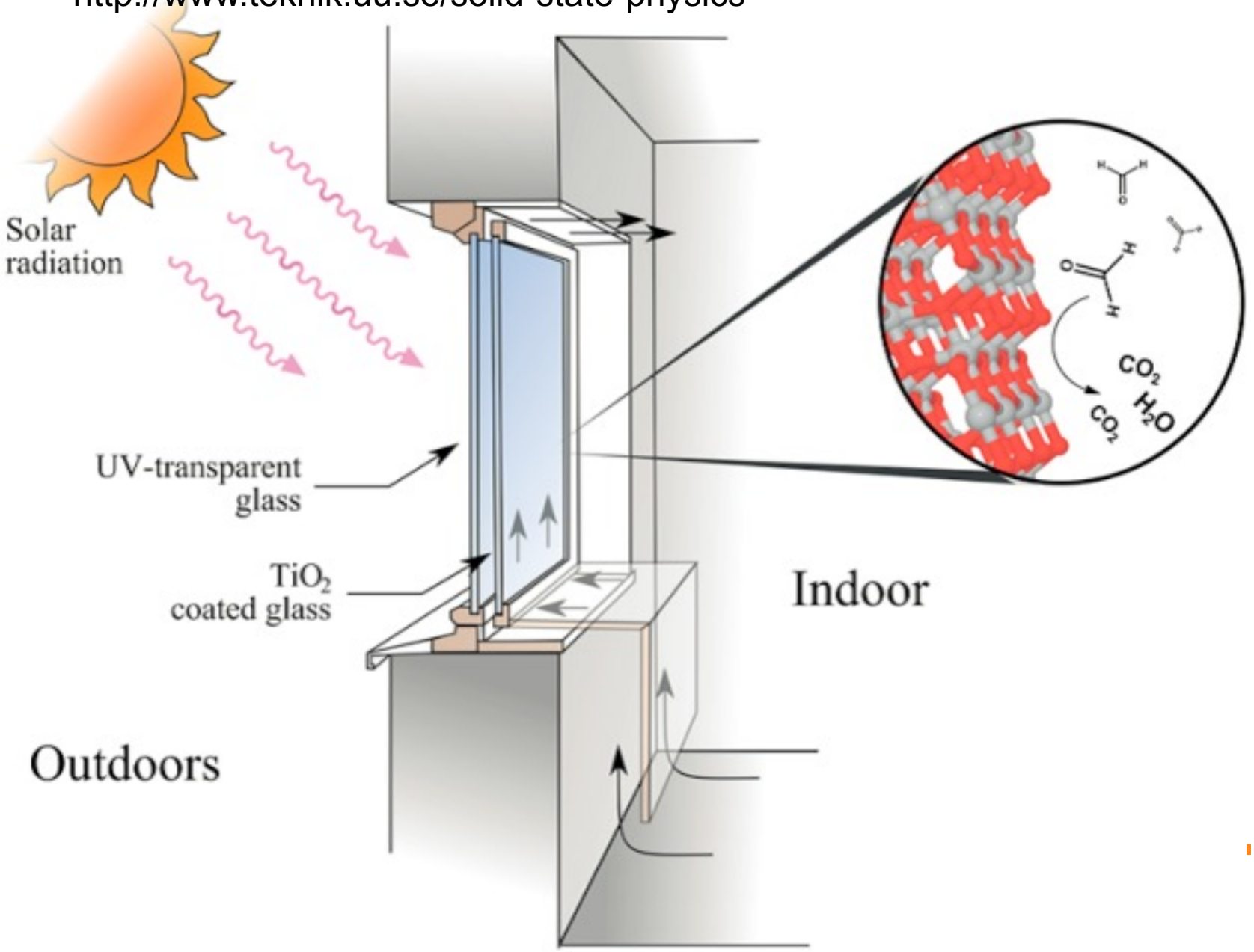

http://www.teknik.uu.se/solid-state-physics

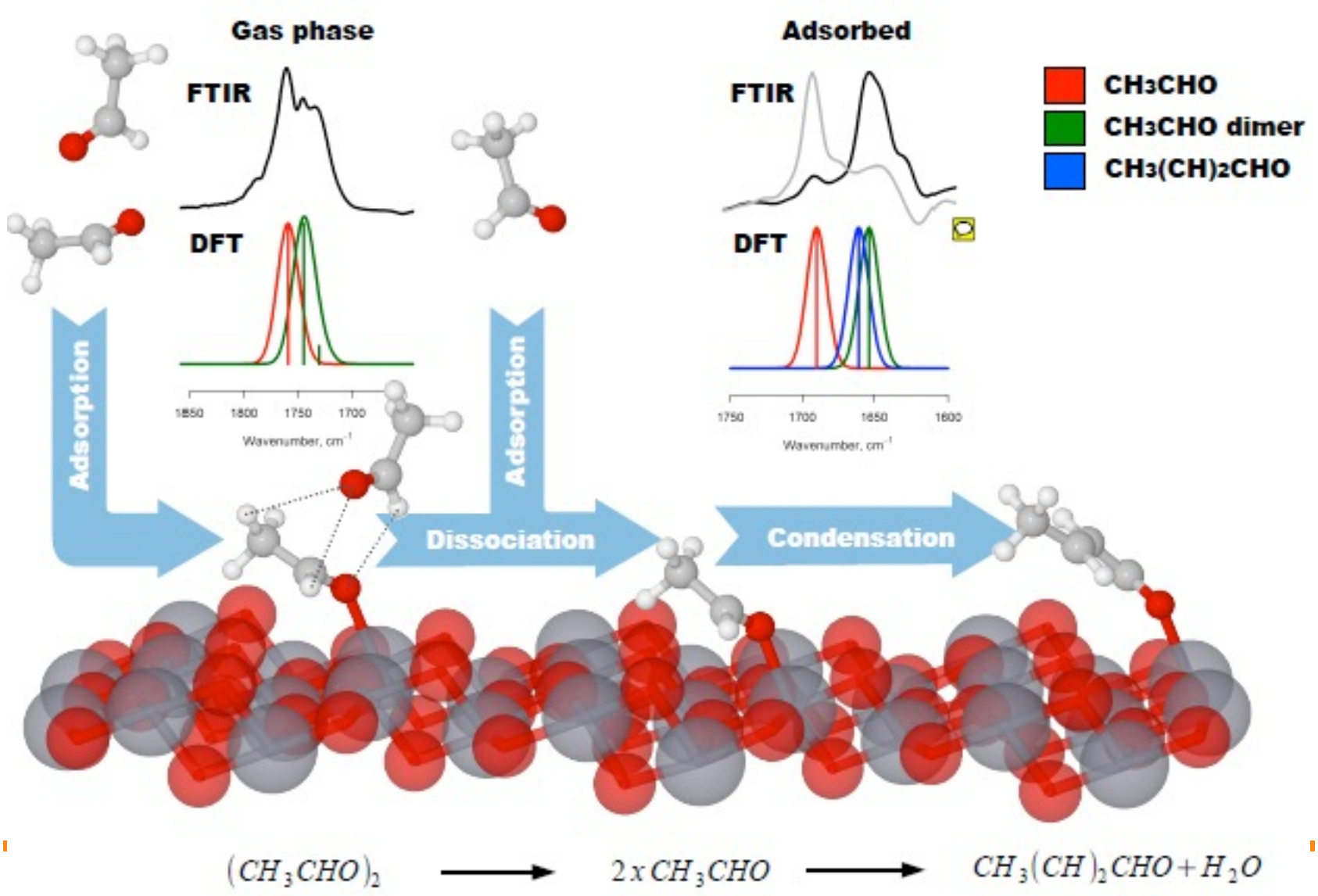

$$(CH_3CHO)_2 \longrightarrow 2x\,CH_3CHO \longrightarrow CH_3(CH)_2CHO + H_2O$$

Measured and modeled reaction kinetics of the adsorption and decomposition of acetaldehyde on TiO_2.

Batteries

IoT, MEMS, CMOS memories, Medical implantable	Smart cards, Skin patch, RFID	Wearables, E-textile, Medical device	Smartphone, Tablet, Power tool, Toy	Transport	Large-scale energy storage
Capacity range →					
1 mAh	10 mAh	100 mAh	1 Ah	100 Ah	> 1 kAh
Important features					
• Rechargeable • Small footprint, many micro-batteries • Long life time • Rapid discharge • Tend to incorporate with energy harvesting	• Can be both disposable and rechargeable • Laminar and thin, some with special form factor • Relatively low power • Cost sensitive	• High energy density for small volume • Long working hours • Flexible, stretchable or thin, some with special form factor	• Light-weight and small volume • Long working hours • Some with special form factors • High power	• Safe • Reliable • High power • High capacity	• Cost advantage • Long life time • Reliable • High capacity
					
Technology Status					
Small volume production	Available, mostly customized	Prototypes available	Research to prototype	Research	Very early stage

https://www.idtechex.com/research/reports/flexible-printed-and-thin-film-batteries-2019-2029-0006

Wearable electronics by ALD

- Prof. Maarit Karppinen group

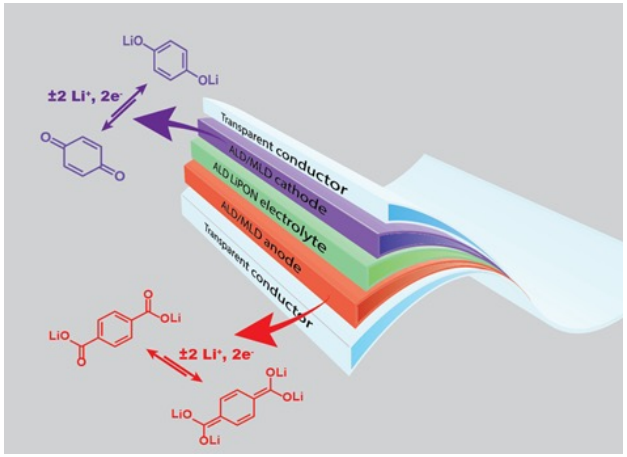

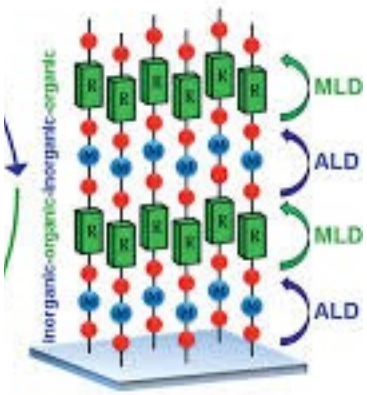

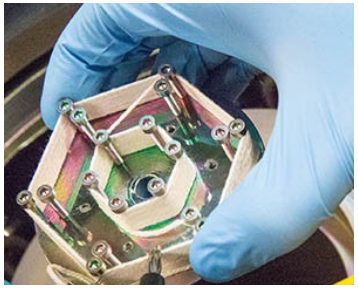

And numerous other functional thin films

- Bio-active, bio compatible
- Controlled (drug) reliese
- Stimulus-responsive
- Magnetostrictive
- Piezoresistive
- etc.